Doctoral Dissertations and Master's Theses

Spring 3-2017

Computational Modeling of Thoracic Injury Response due to Impact of a Small Unmanned Aerial System (SUAS)

Alexander Fumiyoshi Dori
Embry-Riddle Aeronautical University

COMPUTATIONAL MODELING OF THORACIC INJURY RESPONSE DUE TO
IMPACT OF A SMALL UNMANNED AERIAL SYSTEM (SUAS)

by

Alexander Fumiyoshi Dori

A Thesis Submitted to the College of Engineering Department of Mechanical
Engineering in Partial Fulfillment of the Requirements for the Degree of
Master of Science in Mechanical Engineering

Embry-Riddle Aeronautical University
Daytona Beach, Florida
March 2017

COMPUTATIONAL MODELING OF THORACIC INJURY RESPONSE DUE TO IMPACT OF A SMALL UNMANNED AERIAL SYSTEM (SUAS)

by

Alexander Fumiyoshi Dori

This thesis was prepared under the direction of the candidate's Thesis Committee Chair, Dr. Feng Zhu, Assistant Professor, Daytona Beach Campus, and Thesis Committee Members Dr. Eduardo Divo, Associate Professor, Daytona Beach Campus, and Dr. Victor Huayamave, Visiting Assistant Professor, Daytona Beach Campus, and has been approved by the Thesis Committee. It was submitted to the Department of Mechanical Engineering in partial fulfillment of the requirements for the degree of Master of Science in Mechanical Engineering
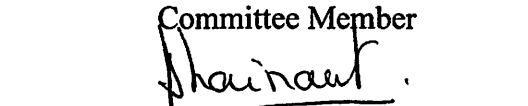
Thesis Review Committee:

_____
Feng Zhu, Ph.D.
Committee Chair
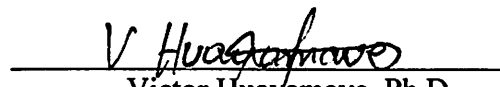
_____   _____
Eduardo Divo, Ph.D.   Victor Huayamave, Ph.D.
Committee Member   Committee Member

_____   _____
Jean-Michel Dhainaut, Ph.D.   Charles F. Reinholtz, Ph.D.
Graduate Program Chair,   Department Chair,
Mechanical Engineering   Mechanical Engineering
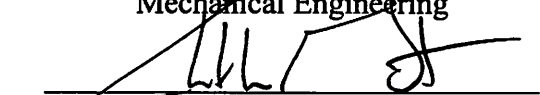
_____   _____
Maj Mirmirani, Ph.D.   Christopher Grant, Ph.D.
Dean, College of Engineering   Associate Vice President of Academics

_____
4/12/17
Date

i

Acknowledgements

I would like to thank my mother, sister, and my late father for supporting me and always being there for me during challenging times. None of this would have been possible if it was not for the constant support and motivation you guys have provided over the years.

I would like to recognize Rebecca Gold in helping me revise and edit my thesis at every step. If it was not for your help, this paper would sound like a toddler wrote it, since my English writing skills are not up to par. I would also like to thank (future Dr.) Arka Das as well for checking the content of this paper as well. I am extremely appreciative of all the help and support you have given me over the past few months. My family and I are very thankful for all of your help.

I wish to gratefully thank my supervisor Dr. Feng Zhu for the support and guidance he has provided throughout this research. Without your wisdom, academic guidance, and moral support, I would not be able to finish this project.

I would also like to thank (future Dr.) Xianping Du for all of the assistance and guidance that you have helped me with. I know I would constantly ask you similar question over and over again, but thank you for being so kind, understanding, and available each time to assist me. I really do appreciate it.

Lastly, I would like to thank Dr. Eduardo Divo for initially getting me involved into Project ASSURE (Thank you for partially supporting this project). From the bottom of my heart, thank you for all the administrative guidance and assistance that you have provided in the past few years. I really appreciate it and thank you.

Abstract

Researcher: Alexander Fumiyoshi Dori

Title: Computational Modeling of Thoracic Injury Response due to Impact of a Small Unmanned Aerial System

Institution: Embry-Riddle Aeronautical University

Degree: Master of Science in Mechanical Engineering

Year: 2017

This study aims to establish a computational model that will predict the injury response after a sUAS impacts the thorax. A rotary and fixed winged sUAS were chosen for analysis. A vast number of numerical simulations were carried out with varying masses, impact velocities, and impact angles. From the simulation results, the maximum viscous criterion was then calculated. A nonlinear surrogate model was established by setting the impact parameters as independent variables and the viscous criterion as the dependent variable. A correlation analysis showed the impact velocity and angle to significantly influence the results more, when compared to the mass. The surrogate model was then tested against randomly selected cases and showed to have good agreement. The highest percent difference was *9.49%*. Simulating a wider range of masses can improve the validity of this model. The surrogate model would become useful in estimating the maximum viscous criterion for possible injury responses.

Table of Contents

List of Tables

List of Figures

Nomenclature

List of Acronyms

AIS	Abbreviated Injury Scale
AMVO	Anthrometry of Motor Vehicle Occupants
ATD	Anthropometric Testing Device
BC	Blunt Criterion
CDC	Center of Disease Control
FE	Finite Element
FEA	Finite Element Analysis
FUFO	Full Fusion Option
HG	Hour Glass
IPR	Injury Priority Rating
ISS	Injury Severity Scale
LNLL	Lawrence Livermore National Laboratory
LSTC	Livermore Software Technology Group
PDE	Partial Differential Equation
PMHS	Post Mortem Human Subject
PODS	Probability of Death Score
ODE	Ordinary Differential Equation
RAMSIS	Rechnergestiiztes Antropologisch-Matchematisches System zur Insassen-Simulation
RC	Remote Control
sUAS	Small Unmanned Aerial System
VC	Viscous Criterion

Chapter I: Introduction

1.1 Motivation

In recent years, Unmanned Aerial Systems (UAS) has been gaining enormous amounts of popularity in almost every business industry. Small Unmanned Aerial Systems (sUAS) are especially popular in military, cinematography/photography, academic, and recreational use. They are used to perform various tasks such as reconnaissance, object following, and filming action scenarios, just to name a few. Regardless of the use, if the sUAS strikes a person's chest there is possibility that it may injure a person or be fatal.

Impacts between a rotary/fixed wing sUAS and a thorax of an Anthropomorphic Testing Device (ATD) will be the main focus. A physical test with cadavers will be able to provide more useful data and give a better injury response but the cost of cadaver testing is quite expensive, and the data is highly scattered. Instead, a numerical simulation will be conducted using a finite element crash test dummy, or ATD, to save cost and time. An ATD will be used as a surrogate since it is readily available to download from Livermore Software Technology Corporation (LSTC) and have been used in many impact studies in automotive safety. The methods used in assessing the injury from an automotive crash will assist in assessing the injuries that may arise from a sUAS and human interaction. An ATD will be much more computationally stable during localized loading conditions when compared to a human model with soft tissues and internal organs. A human model will require specific material properties in order to simulate organ responses to blunt impacts, which may lead to the instability. The Rotary wing

sUAS used is a DJI Phantom 3 quad-copter, which is similar in size of the ATD's chest, shown in *Figure 1.1.*
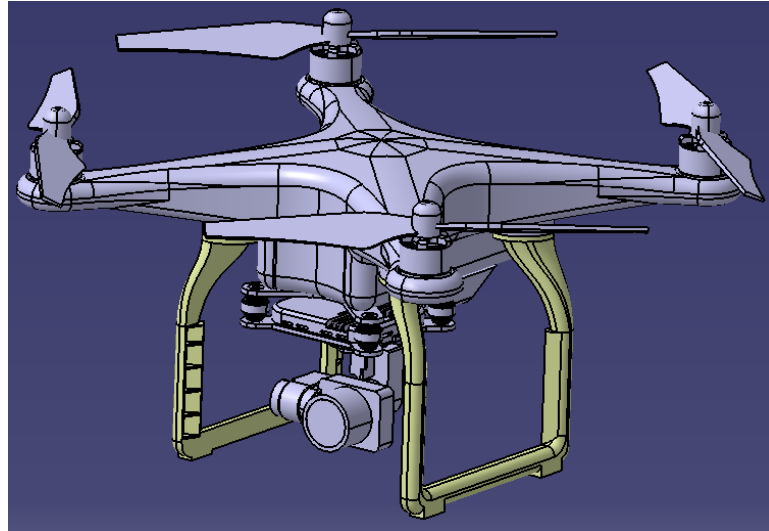
***Figure** 1.1: DJI Phantom 3 sUAS CAD Model used in the simulations.*

The Fixed wing sUAS used is a GZ500 flying wing, which from winglet to winglet is no longer than the arm-span of the ATD, shown in *Figure 1.2.* These specific sUAS were selected due to their popularity among the consumer market. The possibility of a chest impact is unlikely, but if it does happen it can be dangerous depending on several key parameters such as impacting speed, angle of impact, weight of the sUAS, and the material of the sUAS itself.
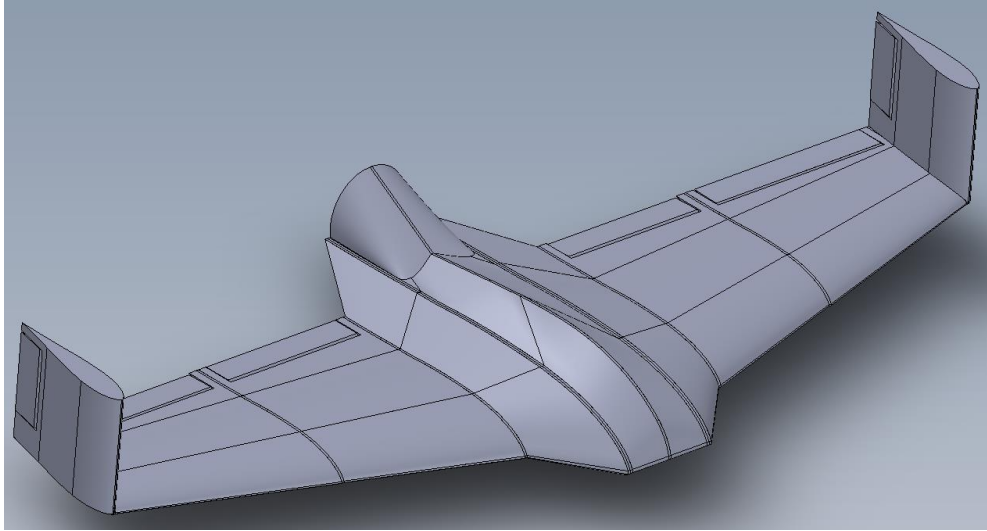
Figure 1.2: GZ500 sUAS CAD Model used in the simulations.

1.2 Background

The number of SUASs flying in our skies has increased exponentially within recent years. Main commercial use for sUAS is to capture amazing videos and photos, and for academic research. The military has a similar purpose, reconnaissance and surveillance from a very high altitude. sUAS are useful, but with enormous amounts of people using these devices, there is bound to be incidents such as colliding with a human and potentially hurting them. During the Madonna di Campiglio in Italy, Marcel Hirscher, a World Cup Champion skier, was nearly hit from a sUAS that was filming his second run in the slalom race [Grez, 2015]. Luckily, the sUAS missed hitting Hirscher. Many of the accidents are from drones falling from the sky due to engine failure, loss of power, or hitting obstacles.

sUAS/human collisions are still considered to be fairly new, therefore, automotive crash testing data and predictors are used to correlate injuries since there is an abundance of this data. Injury to the upper torso (i.e. head, neck, chest, back) is imminent in a

sUAS/human impact. Modeling an impact to the head is quite challenging since there are countless scenarios that may occur causing an injury. The head is capable of flexion, extension, adduction, abduction, circumduction, and rotation. In order to properly model the behavior of the head post impact, all of these motions would have to be considered as well as a combination of these motions. Head and sUAS collisions are similar to that of a general blunt impact problem. These problems have been researched extensively, but thoracic impact injuries have not been. Therefore, focusing on impacts between the chest and sUAS will shed some light on this topic.

The chest is the next vulnerable region since the vital organs are exposed. In fatal/serious automotive collisions, chest injury is considered to be second from a head injury according to the U.S. Center of Disease Control (CDC) [CDC, 2007]. In automotive accidents, the thorax is exposed to many interior components such as the steering wheel, dash, and the restraint system. These components may come in contact with the thorax at any point during the collision. The back of the body is not considered since the seat protects it during automotive impacts. In sUAS impacts, posterior body wall is much thicker than the anterior since the thickness would include the spine, scapula, and the musculature surrounding it. The added thickness would provide additional protection from a deep blunt impact [Sturdivan et al., 2004].

1.2.1 Anatomy of the Thorax

The upper torso consists of many regions as stated earlier. It contains the head, neck, chest, back, and abdomen. To clearly show the division of the regions, *Figure 1.3* is provided. This will properly show which body part belongs to which region.
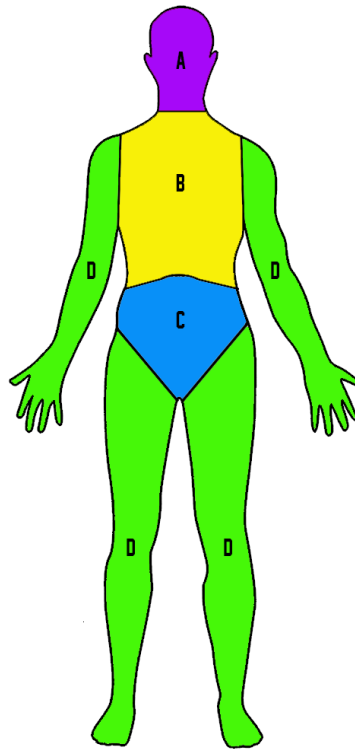
Figure *1.3: Portioned Body Regions.*
Different letters and represent the separate regions of the body,
(A) Head, (B) Thorax, (C) Abdomen, and (D) Limbs (Arms and Legs.)

The thorax contents are separated from the abdomen contents by a thin muscular sheet called the diaphragm. The contents themselves are as follow: the heart, lungs, mediastinum, and the ribcage. The injuries that will be experienced within the torso are separated into internal organ injuries and ribcage injuries. Internal organ injuries occur when the impacting force of the object surpasses the ribcage and causes damage to the organs themselves. Therefore, we will only be analyzing the ribcage compression that is

caused by the sUAS when impacting the thorax. Using current injury surrogate models from automotive crash testing, the injury that will be sustained by the body can be predicted.

The rib cage consists of *twelve* pairs of ribs, which are connected to the thoracic vertebrae posteriorly and to the sternum anteriorly. The first *seven* ribs connect to the sternum at the Chondro-Sternal Junction. Ribs *eight-to-ten* have cartilaginous attachments to the *seventh* rib. Ribs *eleven* and *twelve* are floating ribs, meaning they have no attachment to the sternum or any other skeletal structures [Yoganandan et al., 2015]. *Figure 1.4* is provided to show the structure of the ribcage. The numbers shown correspond to the anatomy as described above.
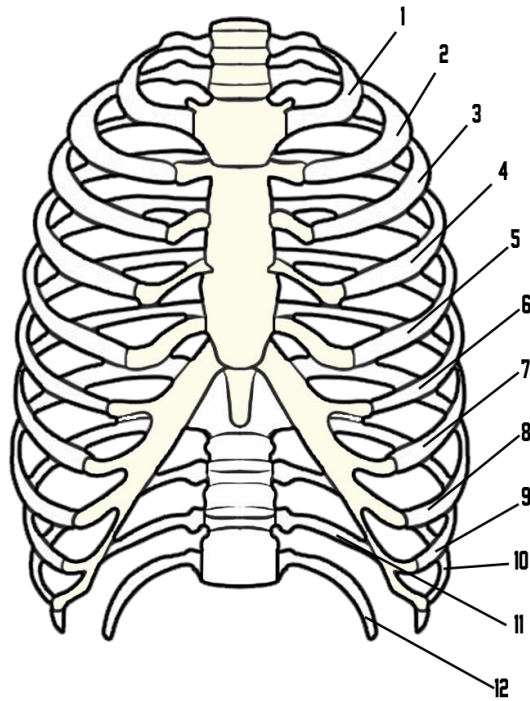
Figure 1.4: Basic anatomy of the ribcage anteriorly.

1.3 Existing Injury Assessments

Predicting the injury level that a person will experience is a challenging task. There are countless numbers of factors that play a role such as, velocity of the projectile, chest compression, age, physical health, impact location, etc. When constructing an Anthropomorphic Testing Device (ATD) for crash testing, many of these factors cannot be accounted for such as the health and age of the victim, because everyone is unique in their own right. Meaning predicting injury for each person becomes a challenge but is not impossible. For instance, material selection is quite challenging when simulating an impact. Selecting the correct material to mimic the human flesh is known to be quite difficult, due to the nature of our bodies. There are layers and layers of muscle along with organs with different material properties that makes predicting injury levels difficult. However, Post Mortem Human Specimen (PMHS) experimental testing can actually help predict the injury levels through observation and measuring impact parameters. PMHS has similar material properties to that of the living; therefore rough injury predictions can be produced.

The following sections describe the existing injury assessments that are widely used in the automotive industry to assess the victim's injury. These injury assessments utilize both a qualitative and quantitative criteria when predicting the injury risks. A comparison of these scales will help select the correct criteria for the impact scenario.

1.3.1 Injury Severity Score (ISS) and Abbreviated Injury Scale (AIS)

If a patient has experienced multiple injuries, the Injury Severity Score (ISS) is used. The ISS is an anatomical based scoring system used to provide a medical score to evaluate trauma severity to a victim with multiple injuries with an overall score. The ISS divides the patient's body into five separate regions:

- **Head & Neck:** Head, Neck, and Cervical Spine

- **Face:** Eyes, Nose, Mouth, Ears, and the Facial Skelton

- **Chest:** Diaphragm and Thoracic Spine

- **Abdomen:** Pelvis Contents, Abdominal Organs, and Lumbar Spine

- **Extremity:** Pelvic Girdle and Legs

Then the Abbreviated Injury Scale (AIS) is used to assess each injury for that particular region. AIS is an anatomical based scoring system that was created by the Association for the Advancement of Automotive Medicine and was introduced in 1969. This scale has been revised and updated since its introduction to provide a much more accurate ranking of injury severity. The most recent major update was last updated in *2008*. AIS is based on a scale from *one* to *six*, with *one* being minor injury and *six* being "un-survivable." AIS *six* is currently untreatable and is not an arbitrary ranking for fatal injury, but instead is a ranking for injuries that are fatal to the victim. An AIS value of *nine* is used to describe any injuries that do not provide enough information for the AIS ranking. *Table 1.1* shows the basic AIS ranking [Copes et al., 1989]. *Table 1.2* shows a summary of different levels of injuries that may be associated from a blunt impact. The

table shows rib fractures and thoracic organ injuries, along with the correlating AIS ranking. The table will also show the correlating chest compression percentage and the viscous criterion value associated with the injury [Fundamentals, 2017].

Table 1.1: Abbreviated Injury Scale

AIS Score	Injury
1	Minor
2	Moderate
3	Serious
4	Severe
5	Critical
6	Un-survivable
9	Not Specified

Table 1.2: Ribcage and Thoracic organ injuries and the associated AIS levels.

Injury Levels		Level 0 No Injury	Level 1 Minor Injury	Level 2 Major Injury	Level 3 Severe Injury	Level 4 Potentially Non-survivable
Frontal Rib Fracture	**Tolerance Level**	No Fracture	1 Rib Fracture	2-3 Fractures	Flail Chest	Flail Chest
	AIS Score	AIS 0	AIS 1	AIS 2-3	AIS 4	AIS 4
	Chest Deflection (mm)	<58	58 – 70	70 –92	> 92	>93
	Chest Compression (%)	25	30	35	40	40
Thorax Internal Organ Injury	**Tolerance Level**	No Injury	Very Minor Contusions	Minor Lacerations	Major Lacerations	Potentially Non-Survivable
	AIS Score	AIS 0	AIS 1	AIS 2-3	AIS 4-5	AIS 6
	Viscous Criterion (m/s)	<0.5	0.5 – 0.75	0.75 – 1.0	1.0 – 1.5	>1.5

To produce an ISS, only the highest AIS score is used for that particular region. Only the top three regions that have experienced the most severe injuries will be used to square their scores and be added together to produce the overall ISS score. *Table 1.3* shows example ISS Calculation table. ISS only ranges from *0* to *75*. An AIS value of *six*

in any region is considered *"un-survivable"* and to proceed with any medical care in preserving life will be pointless. So AIS of *six* may indicate a suspension of medical care for the patient. If a patient is assigned an ISS of anything above *75*, they are automatically assigned to *75*. The ISS correlates linearly with hospitalization, mortality, mobility and other measures of severity after trauma [Barker SP et al., 1974].

Table 1.3: Example ISS calculation table.

Region	Injury Description	AIS	Top 3 Squared
Head & Neck	No Injury	0	
Face	No Injury	0	
Chest	> 3 Fractured Ribs	3	9
Abdomen	Complete Ruptured Spleen	5	25
Extremity	No Injury	0	
External	No Injury	0	
ISS Score:			34

There are some errors associated with this score. If there were any error associated with the AIS scoring then that would propagate to the ISS accumulating error. This is not a weighted scale; therefore, many different combinations of injured regions may yield to the same ISS, which may not be entirely correct. This scale should not be used as a triage tool since a full description of the patient's injuries is not known prior to scoring [Barker SP et al., 1974].

1.3.2 Probability of Death Score (PODS)

Probability of Death Score (PODS) or PODSa (accounting for age) was developed similar to the ISS. The main difference between these two predictors is that ISS shows the probability of survivability where PODS/PODSa shows probability of death as it states in the name. *Equation 1.1* shows the basic expression for PODS and PODSa.

$$PODS = \frac{e^x}{(1 + e^x)}$$

(1.1)

where x is:

For PODS:

$$x = 2.2(AIS_1) + 0.9(AIS_2) - 11.25 + C$$

(1.2)

For PODSa:

$$x = 2.7(AIS_1) + 1.0(AIS_2) - 15.4 + C + 0.06(Age\ of\ Patient)$$

(1.3)

AIS_1 and AIS_2 are the highest and second highest AIS. *C* is *-0.764* for automobiles [Somer, 1983]. PODS/PODSa has a better coefficient of determination (R^2 *value*) compared to the ISS. This predictor also has a better understanding of the health outcome, making it a much desirable score to use.

PODS, AIS, and ISS were developed considering the '*threat of life*' as a main driving factor. If additional factors can be used to assess the injury, such as quality of life or societal cost, then Injury Priority Rating (IPR) and HARM can be used. IPR is able to distinguish impairments that may be associated with the sustained injuries even within the same AIS values. IPR also provides a post accident survival rating [Carsten et al.,

1984]. The HARM concept is used to help mitigate a varying economical cost when treating the patient's injuries. AIS does a great job in evaluating the injury severity, but does not consider the long-term consequences associated with the injury. By assigning an economical cost to an AIS value, it eliminates the variations in cost per injury [Ambrosio, 2001]. This method is useful when calculating the cost of injury from the AIS value, but also has a limiting use.

1.3.3 Compression Criteria

After analyzing large quantities of blunt impact data to the thorax, Kroell et al. found that there is a linear relationship between AIS and chest compression. The blunt impact data were performed throughout the 60's and 70's using a PMHS, in order to improve their comprehension of the thoracic impact response and injury tolerances. The authors recognized that the global acceleration and force could be used to evaluate the body's motion; this would be ineffective predictor of risk in a localized area. Evaluating the global acceleration and force actually neglects the local loading experienced by the body. For instance, the whole body acceleration is negligible for a front impact pendulum test, but the injury that is experienced is very severe. Therefore, using the chest compression is found to be a more suitable predictor for injury risk. Using regression techniques, AIS and chest compression have a correlation value, *R*, of *0.730.* With this being said the maximum plateau force did not correlate well with AIS, having a correlation value, *R*, of *0.524* [Kroell et al., 1974]. The linear expression between AIS and the chest compression is shown in *Equation 1.4.*

$$AIS = -3.78 + 19.56C$$

<div align="right">(1.4)</div>

Equation 1.4 essentially predicts the AIS level by using the chest compression divided by the chest depth, *C*, which can be measured. The authors also found that when *C* is *30%* (*C=0.3*), it correlates to an AIS value of *2*; if *C* is *40%* (*C=0.4*), it will correlate to an AIS value of *4*. This way, the AIS value can be relative to the actual chest compression rather than having a set value for the general public.

Using the same experimental data, Viano and Lau conducted a logistic analysis in order to construct a more extensive injury tolerance level. This study showed that a chest compression of *35%* correlated to an AIS value greater than or equal to *4* with a *25%* probability and a chest compression of *37.86%* correlated to an AIS value greater than or equal to *4* with a *50%* probability [Viano et al. 1988].

Testing shows that to cause a rib fracture a projectile must be traveling *5-7 m/s* and impact the sternum. In PMHS impacts, this speed commonly compressed the chest by *twenty-percent*, which caused rib fractures. A *forty-percent* compression commonly produced a flail chest. A *forty-percent* tolerance will extrapolate to a maximum obtainable compression of *75 mm* to a Hybrid III front impact crash test dummy [Neathery et al.1972].

1.3.4 Viscous Criterion

The vital organs that are essential to our survival are located in the thorax as stated in the previous sections. In order to predict injury risks from an impact, the thorax may not be considered as a rigid structure. In the preliminary stages of injury prediction this may be applicable just for simplicity sake, but will not be completely accurate.

Instead, the body must be considered to be a deformable structure [Viano et al., 1985].
Due to the fact that the chest can be compressed during an impact, the injury criteria
needed for the thorax must consider the compression experienced as well as the rate at
which it is being compressed. *Equation 1.5* shows the expression for the Viscous
Criterion (VC).

$$VC(t) = V(t) * C(t)$$

(1.5)

V(t) is the velocity of the chest relative to the spine, also referred to as the
deformation velocity. *C(t)* is the compression of chest relative to the spine. *V(t)* has the
units of m/s, where *C(t)* is unitless since it is a ratio of the chest compression. *C(t)* is the
chest deformation divided by the unreformed chest thickness, therefore making it
unitless. The previous section stated that the compression criteria can sufficiently
correlate the local chest compression with an AIS value which will in turn show the rib
and soft tissue deformation; it fails to show any rate dependency with soft tissues. In
order to account for the soft tissue rate sensitivity, Kroell et al. explored the effects of
local chest compression and velocity during a blunt thoracic impact. Swine was used
instead of PMHS. The authors showed that a high velocity with a low compression
impact had a greater injury level than that of a low velocity with a high compression
impact [Kroell et al. 1981]. An abdominal impact test was conducted on rabbits to
analyze the effects of a blunt injury. Viano et al. conducted this test and consisted of
variable velocities. The results showed that there was a constant abdominal compression
at both low and high velocities. At low velocities (*8 m/s*), no noticeable injuries were

apparent but at the higher velocities (*20 m/s*) showed minor to multiple liver lacerations [Viano et al., 1981].

Viano et al. again analyzed a large quantity of frontal and lateral impact experiments. These experiments consisted of a wide variety of velocities and thoracic compressions, ranging from *5-22 m/s* and *4-55%* compression, respectively [Viano et al.,1983]. The authors were able to confirm that both the velocity and the compression experienced by the thorax are sensitive tolerances. The chest is able to tolerate 50*%* compression with a *5 m/s* deformation, whereas the tolerance changed significantly when experiencing *20%* compression at *20 m/s*. The data also showed that by multiplying the maximum deformation velocity and the compression experienced by the chest wall produced an effective predictor for injury risk. The viscous criterion is known to be a rate sensitive torso compression that defines the biomechanical index of potential for soft tissues.

The maximum compression of the chest can be used when assessing the ribcage damage for low speed impacts (*V<5 m/s*). For higher speed collisions (*V>5 m/s*), both the deformation velocity (*V(t)*) and the chest compression (*C(t)*) are needed to predict the injury risk. VC is the best indicator for predicting soft tissue injury for deformation velocities of *3-30 m/s* [Viano et al., 1986]. For blunt impacts that have velocities less that *3 m/s*, the compression criteria, shown in *Equation 1.4*, should be used. For impact velocities above *30 m/s*, the loading becomes such a large factor in which neither the compression criteria or VC can be used to predict the injury risk. Based on the Probit Analysis (type of regression used to examine binomial response variables), a VC of *1.3*

m/s yielded to *50%* thoracic AIS value that was greater than *3*, and a VC of *1.0 m/s* yielded to a *25%* thoracic AIS value that was greater than *3* [Viano et al., 1986].
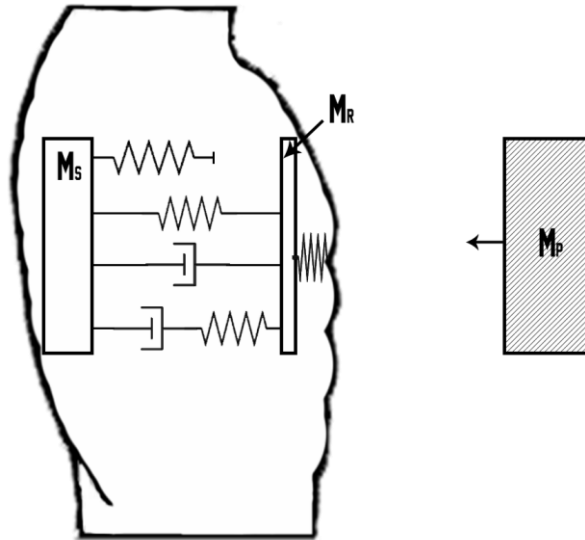
Figure 1.5*: Lobdell's thoracic model.*
M_s is the mass of the spine, M_R is the mass of the ribs, and M_P is the mass of the incoming projectile.

The viscous response (VC) is also known to be a time-varying product of the deformation velocity and the compression of the chest. To further understand the viscous nature of the thorax, Lobdell's thoracic model is shown in *Figure 1.5,* to show mechanical representations for the contents of the thorax [Lobdell, 1972]. This mechanical analogy shown is a biomechanical response of the thorax during a collision. The springs and dashpots in *Figure 1.5* represent parts of the chest. The spring represents the stiffness of the ribcage, which in turn will store the energy during the impact along with the force/compression relationship. This particular stored energy in the spring can show the energy capacity of the chest since the energy capacity is proportional to the compression of the spring itself. The dashpots can simulate the viscous nature of the

thorax. This can show the energy that is absorbed during the impact along with the deformation of the particular element. The maximum dissipated energy (viscous limit) is proportional to VC_{Max} while the maximum stored energy (elasticity) is proportional to the square of the maximum compression, $C(t)$. VC is also a measure of the energy dissipated by the viscous elements in the thorax [Viano et al. 1985].

It is also apparent that the Lobdell thoracic analytical model is comprised of a parallel Voigt and a Maxwell material model. The parallel Voigt material model is the spring and dashpot being parallel to one another. The spring element represents the elasticity of the rib cage and the dashpot represent the soft tissue of the thorax. The Maxwell material model is where the spring and dashpot is in series of one another. This material model shows the viscoelastic element such as the pectoral muscles [Lobdell, 1972].

1.3.5 Blunt Criterion

The original Blunt Criterion for small projectiles impacting a large body is shown in the equation below: [Sturdivan et al., 2004].

$$BC = ln\left(\frac{E}{W^{1/3}TD}\right)$$

$$(1.6)$$

The Blunt Criterion is defined in *Equation 1.6*; where BC is the Blunt Criterion variable used to predict the injury risk, E is the kinetic energy of the projectile at impact in Joules (J), W is the weight of individual represented in kilograms (kg), T is the thickness of the body wall in centimeters (cm), and D is the effective diameter of the projectile in centimeters (cm). When working out the units, it is clear that they do not

cancel each other out, and this is because BC is an empirical equation. This means, any unit will suffice, and will only change the BC value. The authors chose these units to relate the BC to the AIS better.

The expression inside the parenthesis in *Equation 1.6* is an energy ratio. The numerator is the kinetic energy of the projectile impacting the body, which can be thought of as the energy available to produce damage. The denominator shows how much energy the animal or person is able to absorb without damaging vulnerable organs. This expression is dependent on the mass of the body and is scaled accordingly. Scaling the mass is necessary to show the tolerance of the body by the quantity of tissue available. For instance, the amount of damage required to kill a small animal would be tolerable for a human and would be negligible for a large animal such as a rhino. To properly account for the denominator, other physical quantities such as strength and density of tissue must be taken in consideration. These quantities were taken out of the equation and remained constant for all animals to simplify the BC. These physical traits can become curve-fitting constants to relate the BC to the injury level.

Body wall thickness measurements are taken center of the lungs and directly over the ribs. The thickness is approximated by the following expression:

$$T = kW^{1/3}$$

(1.7)

In the equation to calculate the body wall thickness in *Equation 1.7, T* is the body wall thickness, the *k* value for females are *0.59* and *0.711* for males [Radi, 2013], and *W* is the weight of body. The *k* values above are for thoracic impacts because if the projectile would strike the human in the back, it would experience a much thicker body wall.

Since the original BC was formulated for projectiles, which were relatively small in size and mass compared to the body being impacted, the kinetic energy virtually is absorbed by the surrounding impact [Sturdivan et al., 2004]. In our case, the impacting object has a similar size to the body so there will be remaining kinetic energy from the input energy in the following motion of the projectile. However, the residual energy will not distort or cause any damage to the tissue, but must be subtracted from the predicting model. This can be thought of the object bouncing off of the chest, post-impact. By assuming a perfect inelastic collision between the projectile and the body, the effective energy can be estimated. The perfectly inelastic collision will produce the maximum transfer of kinetic energy into potential injury forms. In reality, the object will have a small rebound off of the chest; this assumption will be able to predict most concerns.

In order to predict the effective energy from an inelastic collision, the conservation of momentum is used. Consider a thoracic collision with a sUAS; the sUAS is moderate in size when compared to the chest. During the impact, the body mass used in the equation is the "effective mass" and will move along with the impact. The mass will have a slow transfer in momentum and energy relative to the rate of production of injury. Post-impact, the projectile will become a part of the body conserving the momentum. The derivation is shown in *Equation 1.10.*

$$M_1 V_1 = (M_1 + M_2)V_2$$

(1.8)

$$E = \frac{1}{2}M_1 V_1^2 - \frac{1}{2}(M_1 + M_2)V_2^2$$

(1.9)

$$E = \frac{1}{2}M_1 V_1^2 \left(1 - \frac{M_1}{M_1 + M_2}\right)$$

(1.10)

The variables in the equations above are as follows: E is the energy, M_1 is the mass of the projectile, and in our example it is the sUAS, M_2 is the "*effective mass*" as stated above, V_1 is the velocity of the projectile, and V_2 is the velocity of the combined mass. This modification will generalize the BC to any impact variety.

Modifications will have to be made to the effective diameter variable as well. Since the sUAS is significantly larger than a bullet, the cross-sectional area of the impacting sUAS arm will not be acceptable. For larger objects, an *effective diameter* will have to be calculated, which will show the area of the contact between the projectile and the body. To be considered a *small* projectile, the object must have a radius less than or equal to the impacting body wall thickness. As the object size increases, the area of the contact is dictated by the curvature of the object that is striking the body. An example of this is shown in *Figure 1.6,* where a large sphere is impacting the Hybrid III ATD.
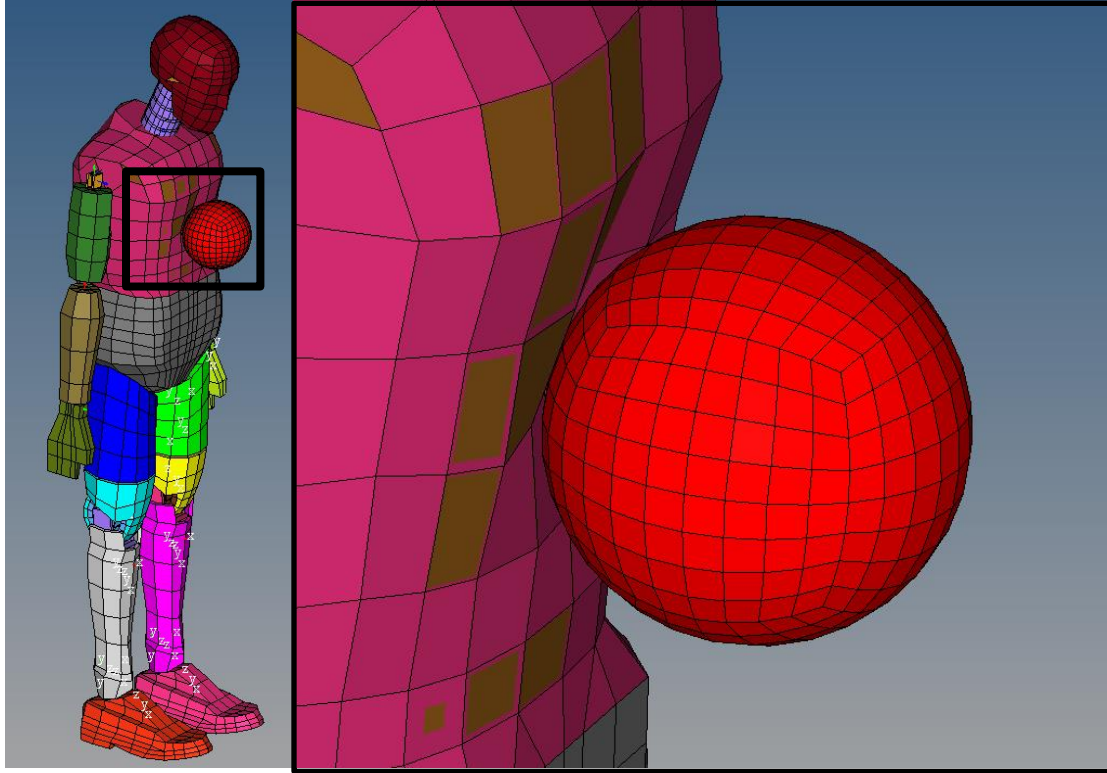
Figure 1.6: *Clearly showing the effective diameter lodging into the dummies chest.*
Left*: Global Reaction from the Ball Impacting the Test Dummy.*
Right*: A close up of the projectile impacting the dummies thorax.*

The effective diameter is derived in the following steps; first find the contact area of the object, then calculate the effective diameter as shown in *Equations 1.11* and *1.12*, respectively, where *D* is the effective diameter that will be used in the BC, *A* is the contact area between the object and the body, *T* is the body wall thickness, and *D'* is the diameter of the object.

$$A = \pi T(D' - T); D' > 2T$$

(1.11)

$$D = 2\sqrt{\frac{A}{\pi}}$$

(1.12)

Effective mass of the body parts will also need slight modification as well. This is a sensitive parameter since this can vary from person to person. In the past, only certain portions of the total body mass were obtained from disarticulated cadavers. Obtaining body mass in this way led to inaccurate approximations of estimating effective mass. The post mortem water loss was not measureable and not correctable either. As new technologies developed, Pignolet et al. suggested a new method of measuring the mass of body parts by determining the mass supported by each vertebra. The experiment consisted of *eleven* women and *seventeen* men, all in good physical condition, and all having normal weight for their height. The data was combined to estimate the effective mass of each body parts. These masses would move independently relative to the neighboring body parts post impact. The results of this experiment are shown in *Table 1.4* [Pignolet et al., 1990].

Table 1.4*: Body Part Proportions for Injury Surrogate for both Men and Women.*

Body Part	Men and Women (%)
Head	N/A
Arm	7
Thorax	21
Mid-abdomen	21
Pelvis	20
Leg	33

It is obvious that when adding the percentages that the total does not equal one hundred percent. This is due to the inaccuracies in the experiment itself, mainly the lower limb portion. Part of the lower limb weight has been transferred to the pelvis. The original data determined the mass supported by the vertebrae ended at the femoral

support. Meaning the authors combined part of the pelvic girdle in with the lower limb when they should have been separated. If there is a full body collision then this would affect the results, but since we are looking at individual body regions, the *effective mass* will remain the percentage shown in *Table 1.4.* The head percentage is also not shown since the body weight percentage cannot be well represented. Head impact is not being considered in this at all, even though the head is highly vulnerable.

Viano et al. similarly derived an estimate of effective mass of the thorax using cadaver data for their impact study [Viano et al.,1989]. In the estimate, there was a large difference in the values, but the averages for each region were close, as shown in *Table 1.4.* It considers that the individual body regions will move as whole together. The discrepancy seen in Pignolet et al. study is apparent here where the lower abdomen will contain the pelvic girdle and will move as unit as well. One other consideration is that there is no skeletal structure in the mid-abdomen area, which makes estimating this region difficult. Even though there is no actual skeletal structure in this area, it is clear that the various organs and the body wall cannot move independently of one another or the spine.

Sturdivan et al. found that there is no statistical difference in the body part portions between men and women in their study. There was only a slight difference in the thorax percentage between the different genders, but was neglected from being a relatively small variance [Sturdivan et al., 2004].

By combining and simplifying the modifications stated above from the following: *Equations 1.6, 1.7, 1.10, and 1.12;* the modified BC for projectiles that are similar in size of the thorax is shown in the expression below:

$$BC = ln\left[\frac{M_1 V_1^2 \left(1 - \frac{M_1}{M_1 + M_2}\right)}{4kW^{2/3}\sqrt{A/\pi}}\right]$$

(1.13)

Equation 1.13 incubuses all of the modifications required for this type of impact, where the projectile is similar in size as the targeted body.

1.3.6 Differences in VC and BC

When analyzing an impact to the human chest there are number of criteria created to predict the injury from the collision. As mentioned in the previous sections, these criterions were formulated using physical measures such as acceleration, force, impulse, and the compression of the body. Both VC and BC are both energy-based predictions. Viano and Lau developed the Viscous Criterion (VC) and are used throughout the automotive industry in crashworthiness [Viano et al.,1985]. VC is used when there is a whole-body reaction rather than a localized one. This criterion is derived from the instrumentation of a dynamic experiment, where BC is derived from physical properties of impacts. VC may be used if the experiment is a global event such as automobile testing or structural collapses. VC assesses the potential injury from an experiment, such as a blunt impact, where the energy input and other factors may not be apart of the BC.

The Blunt Criterion was developed to assess the vulnerability of humans to blunt weapons, projectile impacts, and the behind-body armor exposures within the U.S. Department of Defense. The original BC is better suited for the target body to be much larger than the projectile with low mass and a high velocity (i.e. a bullet impacting a

human). BC would consider the possible penetration that may occur during the collision as well. Modifications can be made to the BC so it can be better suited for larger projectiles, so the object may be similar in size of the target. *Equation 1.13* shows the modified BC, in order for the modification to be effective, every physical parameter must be known. This can become problematic when the projectile has multiple components to it rather it being a single mass object. The modified BC will only augment the local impact area, instead of small area as the BC was originally intended for.

Due to the nature of the two different criterions, VC would be better suited to for a sUAS/ATD collision. As stated earlier, VC is the best predictor when the impact velocity is between *3-30 m/s*. This velocity range will cover the minimum and maximum speeds in which the consumer sUAS will be able to go. In fact, the DJI Phantom *3* used for the sUAS/ATD collision has a max speed of roughly *16 m/s* [DJI, 2015]. For speeds less than *3 m/s*, the compression criteria should be used [Viano et al., 1986]. BC is not applicable since the projectiles, sUAS's, are larger or nearly the same size of the impacting thorax. These physical quantities alone will produce inaccurate results from the BC.

1.4 Biomechanical Responses

Understanding the biomechanical responses of the ATD is very important. Being able to predict the response will ensure a more accurate prediction of the injury severity. Analyzing biomechanical responses can come from several tests, such as the pendulum and sled test that is widely used in the automotive industry. Many of these tests were performed on PMHS under controlled laboratory conditions. These tests were able to

provide measurable biomechanical responses such as deformation, acceleration, and forces. Using these parameters and necropsy post-impact, a detailed injury level were produced, which led to the development of the injury criteria as well as crash test dummies like the Hybrid III. The following sections will show the blunt impact testing and injury that is expected from those tests.

1.4.1 Pendulum Impact

PMHS are used in biomechanical testing to gather biomechanical responses such as forces, accelerations, deformations, and pressures, in order to analyze the resulting injuries through necropsy. PMHS will not provide completely accurate results but will show a good idea of what injuries will be sustained after a body has experienced an impact [Yoganandan et al., 2015]. This analysis of injury is much more realistic than using an Anthropomorphic Testing Device. Within the vehicle crashworthiness realm, pendulum and sled testing are commonly used. Pendulum testing is used predominantly for impact scenarios whereas sled testing is mainly used to test the effectiveness of a restraint system. Sled testing criteria will be neglected since there is no need for this kind of testing in a sUAS/Human collision. From the data that has been collected from these tests, a frontal lateral crash test dummies and injury criteria that can be utilized for more testing has been developed.

Pendulum testing includes a six-inch diameter rigid pendulum impacting the sternum of a PMHS. The data that was collected from this testing shows that an idealized deflection vs. force curve can be derived. This would come from the response of the body and can be categorized in loading and unloading stages [Melvin et al., 1985]. The loading

stage can be broken down to three separate components: (*1*) initial peak, (*2*) plateauing of the force, and (*3*) the maximum deflection. *Component 1* is the peak force that the body will experience when the pendulum is contacting it. This initial stiffness or rapid growth is due to the viscous properties that are within the thorax. *Component 2* is where the force plateaus due to the viscous response of the thorax. *Component 3* shows the maximum deflection of the pendulum. This part is similar to that of an elastic collision, since the two masses (pendulum and thorax) are moving together. The unloading stage is where the impactor starts to come back to its starting location and will detach itself from the thorax; they will be together in the previous component [Yoganandan et al., 2015]. *Figure 1.7* shows an example of the deflection vs. force curve in order to easier understand the body response from the pendulum testing. This is an idealized case. The force and the deflection are dependent on the impact velocity. A slower velocity will yield a lower pendulum force and a higher velocity will yield a higher force output.
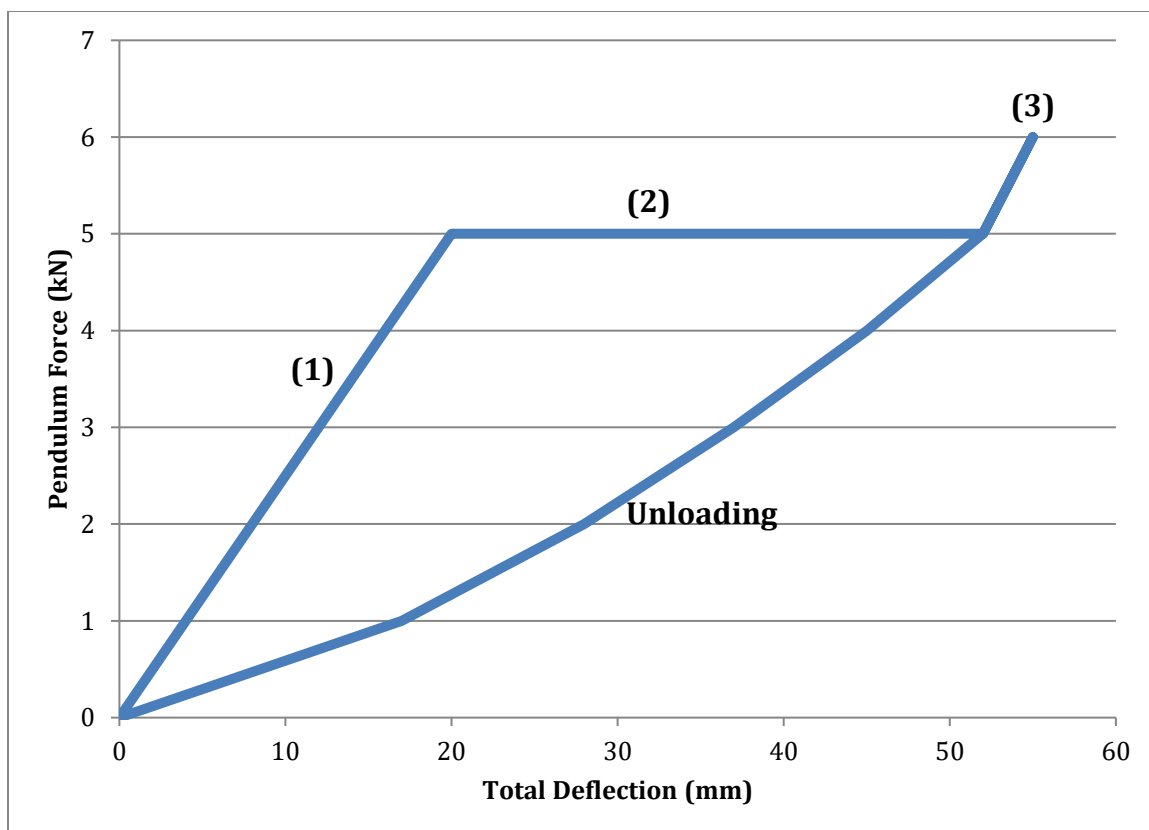
Figure 1.7: Example of an ideal chest Deflection vs. Pendulum Force curve.

1.4.2 Thoracic Injury

When there is a blunt impact to the chest, one of the most common injuries is a rib fracture and a flail chest. A flail chest is a life-threatening condition that occurs when a portion of a rib cage is detached from the chest wall due to trauma. Some common symptoms include shortness of breath and chest pains [Athanassiadi et al., 2004]. As for assigning an AIS value, when there is a unilateral flail chest and *three-to-five* ribs are involved, it is considered to be AIS *3*. When there are more than *five* ribs involved, it is AIS *4*. A bilateral flail chest is considered AIS *5* since this may be life threatening. A rib

fracture can be expected for an AIS *3* value or higher, since the ribcage will be absorbing most of the energy during the impact.

In a cadaver study conducted by Melvin, Mohan, and Stalnaker, it was found that a determining factor for a rib fracture is the maximum compression that is experienced by the chest [Melvin et al., 1975]. Meaning the number of rib fractures is purely dependent on the magnitude of the compression rather than the rate at which it deflects. When reviewing the injuries and the response data, the authors found that rib fractures were much more apparent when the chest depression is over *3 in. (76.2mm).* At the same time, virtually no rib fractures were found with a chest deflection less than *2.3 in. (58.4 mm).* This may seem contradicting since the force applied to the chest is rate dependent. This is caused by the viscous nature of the thorax itself. With that in mind, the force is related to the number of rib fractures depending on a given loading rate.

Chapter II: Model Development

2.1 LS-DYNA

The following sections will explain the LS-DYNA software that was used to conduct the vast number of simulations. The sections will go into detail of how the LS-DYNA calculates the FEM solutions and what parameters were used to set up the experiment.

2.1.1 Brief History

LS-DYNA (Version 971), Commercial software by Livermore Software Technology Corporation (LSTC) was chosen to perform all of the impact simulations between the sUAS and the ATD. This software has explicit and implicit finite element program uses in which explicit time integration is used to analyze nonlinear dynamic problems. LS-DYNA is used in a variety of industries (automotive, military, bioengineering, etc.) to solve various engineering problems. It is important to understand the proper inputs and outputs of this program, along with knowing how LS-DYNA calculates contacts between objects. LS-DYNA originated at the Lawrence Livermore National Laboratory (LNLL) in *1976*, and came from a 3D FEA software called DYNA3D, developed by Dr. John O. Hallquist [LSTC, 2007]. Originally, DYNA3D was created to simulate the impact of a nuclear bomb, called the Full Fusion Option (FUFO) nuclear bomb, when released at low altitude. The original intent for DYNA3D was to analyze stress in structures undergoing a variety of impact loadings. This required significant computer resources and was immediately apparent that speed at which the

software was executing the explicit time integration needed to be updated. To have a gauge of reference, in *1976* the supercomputers were much slower than the common computer of today. [LSTC, 2007]. Due to the computational power at the time, the code was written very simply. The first version of the software contained trusses, membranes, and a few solid elements. The solid elements available ranged anywhere from a one-point quadrature eight-noded elements with hourglass control to a twenty-noded element with eight-integration points. As FUFO got canceled, the development of the software continued. In 1978, the source code of DYNA3D became the public domain per request from France [Benson, 2017].

The *1979* version of DYNA3D was programmed to operate with the CRAY-1 supercomputers. This version contained improved sliding interface treatment and was faster than the previous version's contact treatment by several magnitudes. This version also eliminated the structural elements, solid elements, and higher order solid elements from the first version [LSTC, 2007]. There were many features that were added to DYNA3D during the *1980's*. In the *1982* version, there were nine additional materials that were incorporated to the program. These new materials allowed for new simulations to be conducted, such as soil-to-structure and explosive-to-structure interactions. This update also allowed for the analysis of a projectile that would penetrate an object to be possible. The speed was improved by roughly ten percent as well. DYNA3D acquired many new features in the *1986* version such as beams, shells, rigid bodies, interface friction, discrete springs and dampers to name a few. The program expanded its range as well by expanding to more operating systems such as VAX/VMS, IBM, UNIX, and COS. DYNA3D became the first code to have a generalized single surface contact algorithm

[LSTC, 2007]. The *1987* version brought metal forming simulations and composite analysis possible. More elements and materials were added as well [LSTC, 2007].

Towards the end of *1988* it was apparent that the software would need more development in order to solve problems in crashworthiness. Due to this reason, LSTC was founded by Dr. Hallquist to continue the development of DYNA3D as commercial software, called LS-DYNA3D, shortened to LS-DYNA later [LSTC, 2007]. There has been considerable progress made to the software for further advancement in crashworthiness studies. The list of additions made to LS-DYNA are shown on the LSTC website or in the LS-DYNA user manual. To understand the jargon and the concept of using LS-DYNA, please refer to the Appendix B or the LS-DYNA user manual. Appendix A will show an example of how to solve a simple problem using the finite element method. LS-DYNA will conduct similar steps in solving the more complex problems.

2.2 Numerical Methods

Calculating an analytical solution for real-life problems that are modeled by ordinary differential equations (ODE) or partial differential equations (PDE) are near impossible, numerical methods are used to approximate the solution. There are various numerical schemes on solving these types of equations and in the following sections; differences in the implicit and explicit equations, finite element analysis, and the Galerkin Method will be discussed.

2.2.1 Implicit vs. Explicit

Since LS-DYNA is an explicit and implicit finite element program, it is important to know the differences between the two equations and methods. An explicit numerical scheme is when a direct computation of a dependent variable can be made and *Equation 2.1* shows a simple example of this. Notice that *y* is a dependent variable and is defined by the independent variable *x*.

$$y = x^2$$

(2.1)

An implicit numerical scheme refers to the dependent variables being defined by a set of equations, matrix, or an iterative technique. *Equation 2.2* shows a simple example of this. There are multiple ways to solve an implicit numerical scheme.

$$y - x^2 = 1$$

(2.2)

Both *Equation 2.1* and *2.2* represents the same parabola. Notice that implicit functions can be written as an explicit function. It is often easier to differentiate an implicit function without rearranging the function.

When analyzing both implicit and explicit equations, LS-DYNA will approach this separately depending on the type of analysis, static and dynamic. In a static analysis, the effects of damping or inertia are not present. This kind of analysis can be accomplished through the implicit solver in LS-DYNA. In a dynamic analysis, such as an impact and a crash, the inertia and damping effects are included since they are related to the nodal forces. This type of analysis can be accomplished using either the implicit or the explicit solver [Dynasupport, 2014]. In implicit analysis, the numerical solver

conducts a computationally expensive operation and will invert the stiffness of the matrix once or several times during the current load or time step. For an explicit analysis, this is operation is not required.

If the function requires a nonlinear implicit analysis, then the solution at each step must go through several iterations in order to establish equilibrium, depending on the tolerance. For a nonlinear explicit analysis, it is the opposite of the implicit solver where no iterations are needed since the nodal accelerations are solved directly by taking the inverse of the diagonal mass matrix and multiplying that by the net nodal force vector. This net nodal force vector includes external forces, damping, bulk viscosity, stress, and hourglass control. During the current time n the acceleration is calculated, then the velocities are calculated at time $n+1/2$, and then the displacement at $n+1$. Once this is all calculated, the displacement will show the strain and then the stress can be computed from the strain. This cycle will repeat until the end time. [Dynasupport, 2014] Explicit analysis also handles nonlinearities much easier when compared to the implicit analysis. The nonlinearities would include the treatment of contacts and materials as well.

In an implicit transient analysis, there is no time step size limitation and also allows for a larger time step to be used. For an explicit transient analysis, the time step is limited by the Courant and Fourier conditions [Dynasupport, 2014]. *Table 2.1* will show the difference between the implicit and explicit analysis that were discussed above.

Table 2.1: *Brief summary showing the differences in Implicit and Explicit Analysis*

Implicit Analysis	Explicit Analysis
Implicit Solver solves Static Analysis	Dynamic Analysis can be solved by explicit or implicit solver
No effects of damping or inertia	Damping and inertia effects are included
Inverts the stiffness matrix once or several time during the current load or time step	Nodal accelerations are solved directly and no iteration is required
Several iterations are needed to establish equilibrium, depending on the tolerance	When the acceleration is known t time *n*, then the velocity is calculated at time *n+1/2*, and then the displacement at time *n+1*
No time step size limit	Handles material and contact nonlinearities with relative ease
It allows use of larger time step to be used.	Time step is limited by the Courant and Fourier conditions.

It is apparent that the time step size is crucial for both the implicit and the explicit solvers. Knowing the time step for any simulation is one of the most difficult tasks. Time step size is roughly related to the time it takes for an acoustic wave to pass through an element by using the shortest distance available. In order to determine the new time step (t^{n+1}) for the next iteration; LS-DYNA will loop through the time step through every element. Once the *N* amounts of elements have been looped through, the minimum value will be taken, and be multiplied by a scale factor *α,* to produce the new time step size. *Equation* 2.3 shows the expression used to find the new time step size. For stability reasons, scale factor *α* is used and is set to a default value of *0.90* or smaller. Any value that is larger than *0.90* will lead to instabilities in the solution. If possible, the largest stable time step size will lead to a decrease in solution time [LSTC, 2007].

$$\Delta t^{n+1} = \alpha \min(\Delta t_1, \Delta t_2, \ldots, \Delta t_N,)$$

(2.3)

As stated earlier, the time step size is roughly the speed of sound traveling through a material. This means that it is important to know what material will be used during a simulation. For instance, two materials that are commonly used in the automotive industry are steel and aluminum; sound roughly travels *5000 m/s* or *5 mm/μs* through the material. If the steel structure used had an element size of *5mm* then the computed time step size would be *1 μs* [LSTC, 2007]. *Table 2.2* shows how the speed of sound differs depending on the material. A simple example suggests that elements made with materials that do not allow sound to travel as fast, the time step size will have to be increased. The example showed that with a "reasonable" time step size, the element size, is 5mm; if this was an automotive geometry it could not be represented fully with FE [LSTC, 2007]. It is a balance game between element size, stability, and the time step size, but as computers are becoming more advanced the obstacles are becoming less apparent.

Table 2.2: Different speed of sound in different materials.

Material	Speed of Sound (m/s)
Air	340
Water	1478
Steel	5240
Titanium	5220
Plexiglass	2598

2.3 Surrogate Model for Impact Response Prediction

Once the simulation results have been gathered, a non-linear surrogate equation will be created to predict the relationship between the Viscous Criterion (*VC*) and different impact parameters, such as the impact velocity (*V*), sUAS mass (*M*), and the impact angle (*θ*). This surrogate model solely depends on the input and output parameters of the problem. A Response Surface Method (RSM) approach was selected since it is well established and has been extensively applied to engineering design. This approach is also best suited for applications that have random errors within the system [Simpson et. al., 2001]. Considering there are vast amounts of numerical simulations conducted, it is assumed that there will be random errors. Typically response surfaces are second-order polynomial models but in this case a higher order response surface was used. Instabilities in the model would typically arise from doing this from not having adequate amounts of sample points to estimate the coefficients. In this experiment, this isn't a problem since there are many sample points being taken. The surrogate model can be represented in *Equation 2.4*.

$$VC_{Max} = a + bV + c\theta + dM + eV\theta + fVM + g\theta M$$
$$+ hV^2 + i\theta^2 + jM^2 + kV^3 + l\theta^3 + nM^3$$

$$(2.4)$$

The various combinations of the impact parameters populated the data table for each aircraft to assure that most of the cases were considered. *Equation 2.16* will be curve-fitted in order to determine the coefficients *a, b, c, d, e, f, g, h, i, j, k, l,* and *n*. An general optimization software package known as 1stOPT was used to curve-fit the

function. 1stOPT is based on a Universal Global Optimization algorithm [1stOPT, 2014]. Typically an optimization process will find certain points in order to minimize a function. Global optimization is different from a traditional optimization by finding the maximum and minimum from its inputs rather than finding the local maximum or minimum [Liberti, 2008]. In mathematical programming, a problem can be broken down into two categories, convex and non-convex optimization. Fundamentally, the results of a convex analysis will state that the optimal local solution is also the optimal global solution. It is important to note that after each iteration there is an algorithmic termination test, which tests whether the current solution is locally optimal dependent on the predefined neighbors. For a convex optimization problem, this can ensure that the solution is globally optimal and will be the only optimal solution or there will be no other feasible solution. A non-convex problem is different because there are many different local optima's and is a difficult task to choose the best one from the set [Liberti, 2008].

A Simplex Method algorithm was used for the curve fitting. This algorithm is used to solve problems in linear programming, and will essentially go through a set of feasible solutions, one at a time, until an optimal solution is found, if it exists. Once there is a feasible set or a polytope, the algorithm will test adjacent vertices in order so that the objective function in each new vertex will wither improve or remain unchanged. This method is efficient when in use since it will generally take about *2m* to *3m* iterations (*m* is the number of constraints) and converges in the expected polynomial time (number of steps needed to complete an algorithm for the given input is $O(n^k)$, where *n* is complexity of the input and *k* is a positive integer) for a certain distribution of random inputs [Forsgren, 2002].

The independent (*V, M, θ*) variables were also normalized in order assure that one variable will not overcome another one. *Equation 2.5* shows the expression used to normalize the variables and *Table 2.3* shows the normalization factors used for each variable. The dependent variable (*VC*) was not normalized since it does not affect the curve fitting. If the *VC* were normalized, then the user would have to multiply the *Prediction VC* with the *Normalization Factor* used for the *VC* to get the actual *VC* value. From testing both cases of normalizing and non-normalizing the *VC*, the results and the percent differences were identical.

$$Normalized\ Variable = \frac{|Independent\ Variable|}{Normalization\ Factor}$$

(2.5)

Table 2.3: Normalization Factors used.

Variable	Normalization Factor
V (m/s)	50
M (kg)	2.0
θ (°)	180

Once the surrogate model is created, a correlation analysis will be conducted to analyze the input parameters of the predicted *VC*. To measure the linear dependence between the variables, a Pearson correlation coefficient will be used. The coefficient will have a value between *+1* and *-1*. A value of *+1* is a positive linear correlation, *-1* is a negative linear correlation, and a value of *0* means there is no linear correlation [Correlation, 2017]. The *p-value* will also be calculated to see the significance of the results as well. The p-value will indicate whether the variable has a strong correlation or not. Typically when *p ≤0.05* or (*5%*), this will indicate a strong correlation, if it is greater than *5%* then there a weak correlation [Wasserstein et al., 2016].

Chapter III: Model Development

3.1 Rotary & Fixed Winged Unmanned Aerial System/Vehicle

Current day sUAS's are very diverse in design and can be categorized in many ways. The two most popular types of sUAS's are rotary and fixed wing sUAS's. The rotary winged sUAS's are capable of vertical take off and flight. The kinematics of this type of winged aircraft is similar to that of a helicopter. The main difference is that a helicopter uses two rotors, a main vertical mast and a tail rotor for stability. A rotary winged sUAS needs at least four rotors in order to maintain stable flight. These devices are very nimble, can execute very tight maneuvers and are often utilized in media production.

Fixed winged sUAS's work similar to the classic remote-controlled airplanes. These sUAS's are very popular due to its simplicity when compared to the rotary wing. Design can vary from a flying wing to a glider type aircraft. These devices are predominantly popular in military applications such as surveillance missions.

The preprocessing will be performed using meshing software called Hypermesh by Altair Engineering in Troy Michigan. This software will be used to process the CAD models and convert them to finite element (FE) models to setup the sUAS/Human interaction.

3.1.1 Converting CAD Models to Finite Element Models

Figure 1.1 shows the DJI Phantom *3* sUAS that will be used as the rotary sUAS in the simulations. This CAD model is available to download to the public from a website called *grabcad.com* [Hanmao, 2015]. This website contains various CAD models from users that want to share their drawings. There is no scaling of the obtained models are required since the models have the correct dimensions. The Phantom *3* is approximately *1.3 kg* and has diagonal size of *350 mm*, excluding the propellers [DJI, 2015]. The GZ500 Flying-Wing was also obtained from *grabcad.com* and was designed by Kavian Niazi, shown in *Figure 1.2* [Niazi, 2016]. The Flying-Wing is approximately *2.0 kg* in weight and has a wingspan of *1.214 m*.

In the preprocessing stage, the CAD model will be converted into a FE model to prepare it for simulation. The preprocessing steps include cleaning up geometry, applying mesh, material and properties selection, and boundary/initial conditions. The preprocessing stage is where most of the time should be focused due to the amount of detail is needed for the simulation. *Figure 3.1* and *Figure 3.2* show the converted DJI Phantom 3 and the GZ500 Flying-Wing FE model that were used for the simulations, respectively. The predominate mesh shape used is a quadrilateral in a structured surface mesh with having average size of *5 mm* for both aircrafts to ensure precision. This can be easily seen in *Figures 3.1* and *3.2* as well.
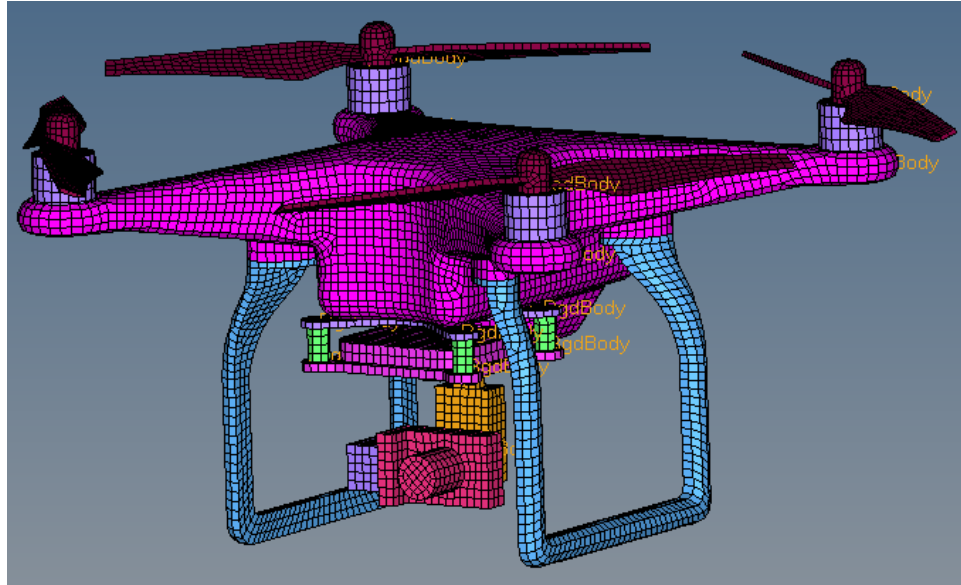
Figure 3.1: *DJI Phantom 3 FE Model*
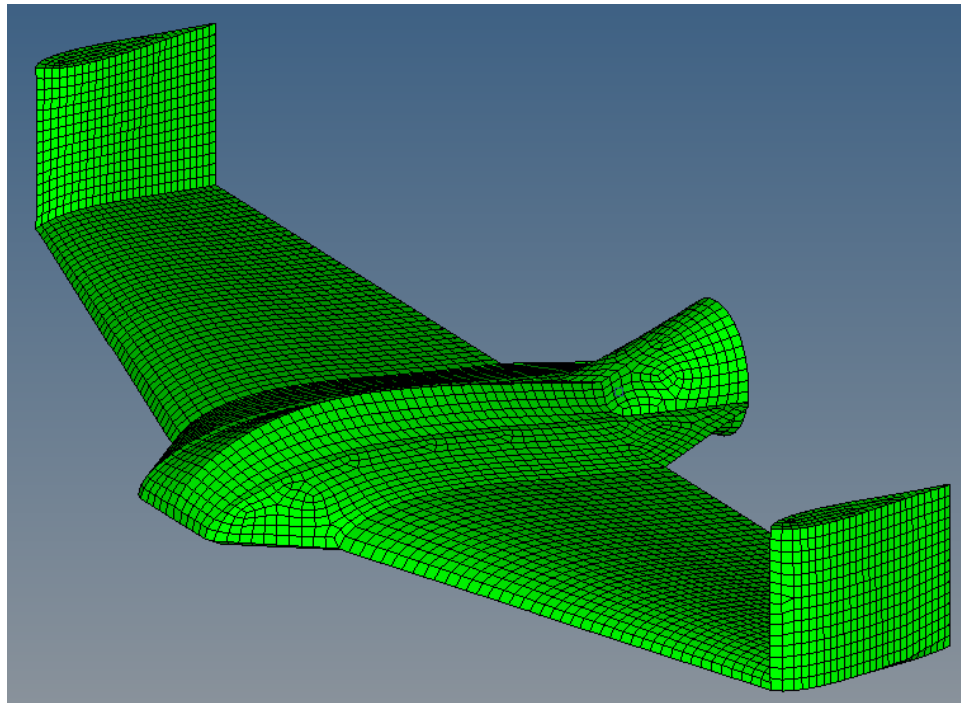
Figure 3.2: *GZ500 Flying-Wing FE Model*

The first step is to clean up the geometry of the CAD model. This can be performed using CAD software, such as CATIA or Solidworks, both by Dassualt

Systemes, or use the meshing software, such as Hypermesh. Once the geometry is cleaned up, the model can be exported in an IGES format, because this format will describe the profile of the sUAS. By comparing the original and FE models, there are significant differences in the features of the sUASs. By eliminating redundant features on the model, this will allow LS-DYNA to perform its calculations much faster, which will cut down on computational time. The redundant features in the Phantom 3 model include things such as rubber grommets for the camera bracket, the ribs in the legs, and the detailed motor design. The redundant features on the GZ500 are minor things, such as the flaps on the wing and the ribs inside the structure itself. Structural support are very important to the sUAS during its operations, but will not be needed during a human impact collision. Since we are only concerned about the response of the human and not the crashworthiness of the sUAS, structural supports were removed.

Once the geometry is cleaned and simplified as much as possible, the next step is meshing. When applying the mesh on the geometry, it is important to keep track of the mesh size and the geometry to perform quality checks along the way. Making the mesh size smaller throughout the model will produce a very accurate result, but will also be taxing computationally. A larger mesh size will show a much more general result and will not be as taxing computationally. Usually a combination of structured and unstructured mesh will be used to construct the FE model; in a wide range of sizes.

The material used for all of the parts on the Phantom 3 and the GZ500 is MATL3 (Keyword: MAT_PLASTIC_KINEMATIC). This is an engineering plastic, which has a typical elasto-plastic behavior. Engineering plastic tend to have better mechanical and thermal properties when compared to common plastics. This plastic has been replacing

traditional materials, such as metal or wood, in certain applications due to its weight and strength. Engineering plastics can equal or surpass the traditional materials in strength and other properties. Generally, engineering plastics are a lot easier to manufacture when compared to the traditional counterparts [IAPD, 2017]. The specific material and property characteristics are shown in Appendix C.

3.2 Anthropomorphic Testing Device (ATD)

In the automotive industry, physical surrogates, such as crash test dummies, are being used for collision instead of humans. These crash test dummies have been designed to predict the human body response that will occur during an automotive collision. These crash test dummies are in constant development so the most accurate human response data can be provided. The validation of these dummies using numerical models is essential in the advancement of the automotive industry. Anthropometric data provides the physical measures such as dimensions and the masses of the various body components. The anthropometric data is important for the development of the numerical models.

For a sUAS/Human collision, an Anthropomorphic Testing Device (ATD, crash test dummy) will be used in place of the human in the crash test simulations. The ATD that will be used is a Hybrid III 50th Percentile. The specific details for this model will be discussed in the following sections.

3.2.1 Anthropomorphic Measurements

Understanding the biomechanical responses of a person after a thoracic impact is crucial, but before that is possible, an accurate anatomical numerical model is needed. Before constructing an accurate depiction of a person, an understanding of how ATD's were developed is important. Anthropometry is used to measure an individual's physical traits such as, height, width, and weight [Moss et al., 2000]. In recent times, this plays an important role in ergonomic designs, clothing, architecture, and industrial designs, in order to optimize products that would require human measurements. Anthropometric data is needed for a numerical modeling application in order to represent the human body model correctly. Theoretically, creating numerical model for each body size and shape with every combination would revolutionize safety design. This is not a feasible option due to time constraints and economical cost that is associated with creating these numerical models. More importantly, the computational cost associated with such model development is substantial. Instead, average measurements are used to develop the crash test dummies. For frontal impacts, there are 5th, 50th, and 95th percentile male dummies available. There are many different kinds of crash test dummies, each designed for specific testing parameters.

Table 3.1: AMVO and RAMSIS anthropometric database summary.

Body Measurements	AMVO	RAMSIS		
		US & Canada	Germany	Japan & Korea
Body Mass (*kg*)	76.7	72.7	79.2	66.6
Stature (*mm*)	1753	1755	1771	1695
Chest Width (*mm*) (*Taken from 10th Rib*)	312	296	308	300

Anthropometric data is obtained through volunteers and currently exists through several databases. The databases typically include the weight and height measurements of the individual then categorizing the information based on the geographic residence, gender, age, and race. There are two automotive databases that provide enough detail in order to develop an ATD, Anthrometry of Motor Vehicle Occupants (AMVO) and Rechnergestiiztes Anthropologisch-Matchematisches System zur Insassen Simulation (RAMSIS) [Moss et al., 2000]. RAMSIS is a mathematical software that predicts the internal and external anthropometric measurements using three key parameters, waist circumference, sitting height and stature. By adding extra parameters, such as age and race, will only improve the data. RAMSIS gathers the data from the following regions, US and Canada, Germany, and Japan and Korea. The AMVO data was used to determine the anthropometric size of the mid-sized 50th percentile dummy. *Twenty-five* adult males with similar stature were chosen to gather all of the data. *Table 3.1* shows the some of the findings from Moss et al., it shows the measurements from AMVO and RAMSIS databases of the *50th* percentile male. For a sUAS/Thoracic impact, we would only require some of these parameters, such as height, weight, and the chest width of the individual. Notably there are slight variations in the data between the different databases [Moss et al., 2000].

3.2.2 Biofidelity

Assuring the use of a Hybrid III will react correctly to a sUAS impact the chest, the biofidelity of the Hybrid III dummy is very important. Biofidelity is the passive human like mechanical behavior that is simulated through a surrogate, in our case the crash test dummy. Comparing the mechanical and kinematic responses between a human volunteer and the crash test dummy can assess this [Kallieris et al., 1995]. The comparison is only valid if the crash test dummy and the human volunteer are exposed to the same impact conditions. Not only do the same conditions have to apply but the same measurement techniques must be carried out as well, to ensure the mechanical response and the biological responses are compared effectively.

The Hybrid III dummy and cadavers have under gone identical collisions by Kallieris et al. The global kinematic behaviors were compared and found slight differences. The acceleration measurements were taken at Th12 between the two subjects. For the trials where the acceleration of the dummy was higher than the cadaver, there was a difference in the acceleration measurements at the Th1 and the sternum [Kallieris et al., 1995]. This would suggest that the torso and torso articulation of the Hybrid III might be stiffer than that of the cadaver.

The deformation experienced by the thorax was measured using chest bands. Backaitis et al. and Kallieris et al. both observed that the deformation observed by the cadaver was almost twice as greater than the Hybrid III deformation. This will result in twice the VC value as well. This can suggest that the Hybrid III thorax is stiffer than the cadavers [Kallieris et al., 1995].

3.2.3 Anthropomorphic Testing Device Finite Element Model

For a sUAS/Human collision, the Hybrid III 50th percentile male dummy will be used, as shown in *Figure 3.3*. This dummy was chosen because it is the most widely used crash test dummy in the world. The dummy is also capable of being used outside of automotive uses as well. The Hybrid III FE model is available to the public to download from the LSTC website. The company specializes in creating both computational and physical ATD's ready to use in a simulation or a car collision. *Table 3.2* will show the total number of finite element (FE) entities needed to construct the ATD model.

These devices are originally intended for vehicle collision testing, but can be used for other impact situations. The Hybrid III crash test dummy is capable of simulating the human responses during an impact. The parameters needed to generate a collision are accelerations, forces, deflections, and moments. As discussed, the biofidelity of any ATD model is vital in order to obtain accurate results. The findings from Kallieris et al. will be taken into account if applicable. Since that study was conducted for automotive testing biofidelity, there is no guarantee that a sUAS will impact the thorax to that magnitude.

Table 3.2: Summary of FE entities used for the ATD.

	Node	Element	Components	Material	Properties
Dummy	7302	4376	125	126	163
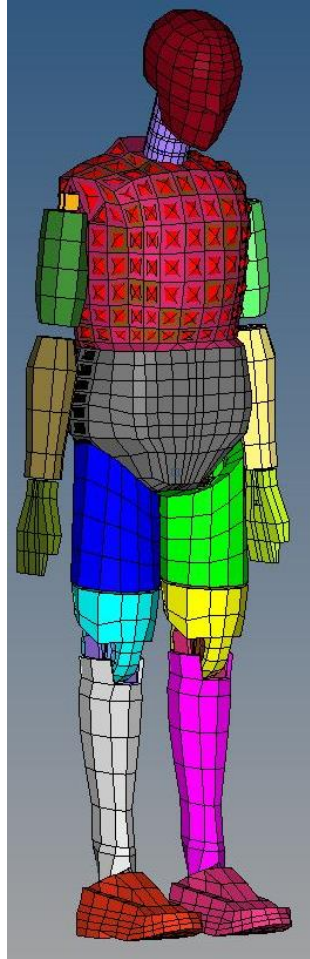
Figure 3.3: Standing Hybrid III 50th percentile Male Crash Test Dummy

3.3 sUAS and ATD Integration

3.3.1 Integration

There are two key parameters that need to be considered in a sUAS/Chest impact, the impact angle (θ) and velocity *(V)*. A suitable impact angle will have a range of *30°* to *90°* [Ball et al. 2012]. The angle measurement is taken from the *Z-Axis,* which runs parallel to the spine, as shown in *Figure 3.4.* The impact velocity can be characterized in two different impact scenarios, loss of control and unexpected descent. When the sUAS

is experiencing unexpected descent, the expected velocity range of this is anywhere from *10* to *15 m/s*. When the pilot has lost control of the aircraft, the velocity can reach up to *30 m/s*. Under normal operation, the sUAS have a max speed of *16 m/s*, and can operate within any range under the max speed [DJI, 2015]. Keeping these considerations in mind, the impact velocity range used was from *5* to *30 m/s*. The impact velocities were increased by *3 m/s* increments. Since the impact velocities can be expressed in two different scenarios, for impact angles *50°* to *90°,* the max velocity used was *26 m/s*. For angles *30°* and *40°*, simulating a loss of control, the max velocity used was *30 m/s.*
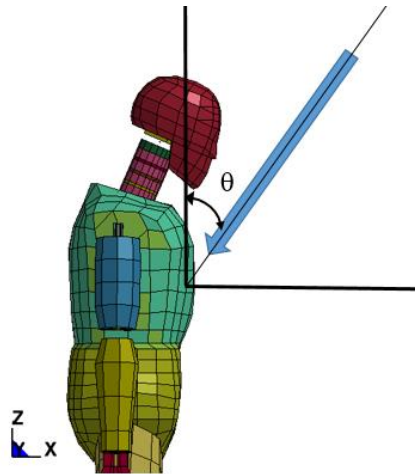
Figure 3.4: Impact angle relative to the ATD.

The FE sUAS model and the ATD were integrated in order to simulate their interactions. *Figure 3.5* shows the integration of both the Phantom 3 and the GZ500 with the ATD, respectively. *Table 3.3* will also show the total number of FE entities used for both cases as well. Both models will start fairly close to the chest in order to save computational time and memory. If there was a large gap between the projectile and the target, then the simulation time will be extended.
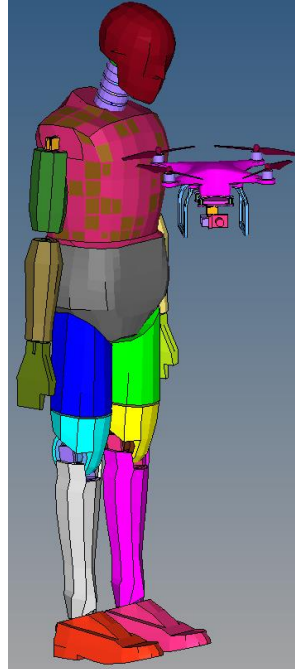
Figure 3.5: *Left: Phantom 3 and ATD Integration Right: GZ500 and ATD Integration*

Table 3.3: *Summary of FE entities used for the ATD/Aircraft integration.*

	Node	**Element**	**Components**	**Material**	**Properties**
Fixed with Dummy	17234	14566	126	126	163
Rotary with Dummy	24323	29703	136	136	173

3.3.2 Contact

From the previous chapter, we know that the main focus of the software is crashworthiness. This means that the contact algorithms are crucial for the prediction capabilities for LS-DYNA. There are many contact algorithms some for specific use and others are common types, such as: Surface-to-Surface, Node-to-Surface, and Single-Surface.

Before contact between two bodies can occur, it is important to note which geometry (node, element, component, set, segment, etc.) will be the slave and which will be the master [Contact, 2012]. Once the slave and master components have been

identified, it is crucial to check for initial penetration, as shown in *Figure 3.6.* Initial penetration is when a body of object 1 is penetrating object 2 before the simulation. This can cause the simulation to be unstable when the simulation is running and may crash within a few time steps. LS-DYNA will try and correct the geometry by moving the penetrating node to the master surface during the first iteration. This in turn may alter another contact surface. To avoid this, geometry should be modified, but keep in mind that some geometry will be more troubling than others.
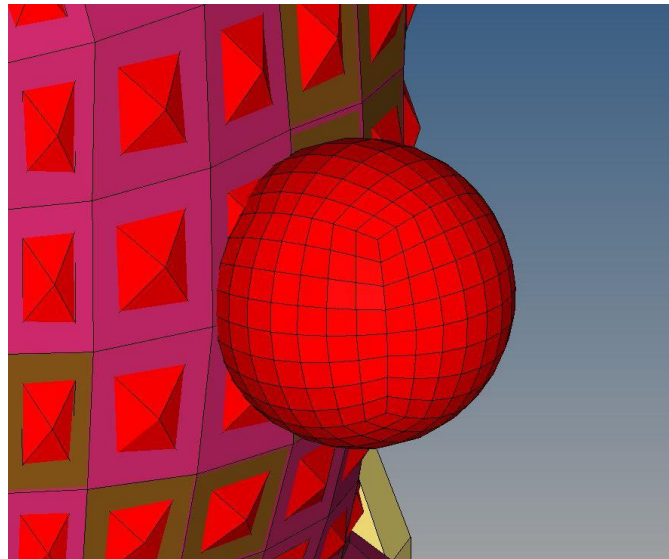
Figure 3.6: Initial penetration of a ball penetrating the ATD chest.

Once there is no initial penetration, the program will search for penetration at every time step through its multiple algorithm depending on what the user has defined. *Figure 3.7* shows some contacts that are commonly used in simulations.
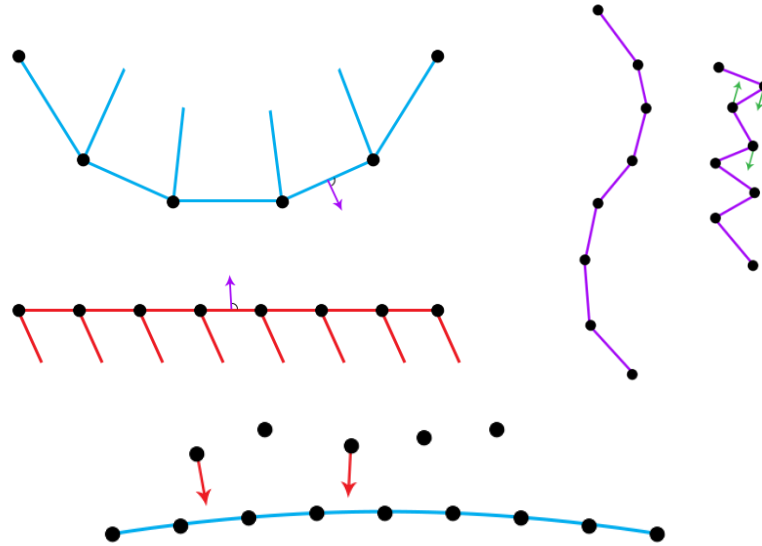
Figure 3.7: *Contact Examples.*
Surface-to-Surface Contact (Top-Left), Single-Surface Contact (Top-Right), and
Nodal-to-Surface Contact (Bottom-Middle)

A surface-to-surface contact is a two-way treatment of contact. First the slave

nodes will be checked for penetration, then the master nodes will be checked for

penetration through the slave segments. The orientation of the shell segments normal is

also important for this type of contact [Contact, 2012]. *Figure 3.8* will show a

representation of this in Hypermesh. The red shading that is shown in the figure is

denoted as the master component and the blue shading is the slave element. In a single-

surface contact, the slave surface is defined, but the master surface is not. The contact is

considered between all of the parts in the slave list. This contact is very accurate, reliable,

and can perform self-contacts, but if there is any initial penetration then the energy

balances may show a decay or growth of energy as the calculation is conducted. This

contact can also be time consuming for the CPU [Contact, 2012]. A node-to-surface

contact is a one-way treatment of contact and a slave node is checked for penetration

through any master segment. This contact can also be used for deformable bodies such as

when there is a fine mesh (slave) element confronts a coarse mesh (master) element [Contact, 2012].
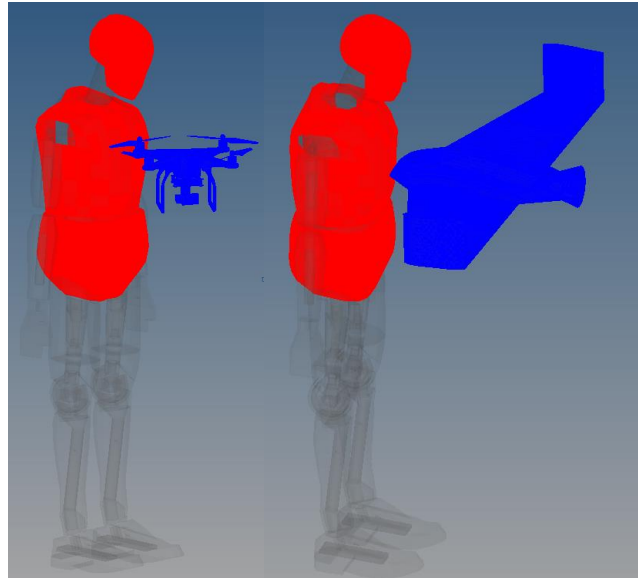
Figure 3.8: Surface-to-Surface contact boundary condition.
Blue denotes the slave component and the Red denotes the master component.

If more problems do persist in simulating a contact, there are some corrections that may help. The slave surface should have a much finer mesh than that of the master. If the slave meshes do have similar densities then the slave surface should have a softer underlying material. On the other hand, if the materials are similar then the slave surface should be the curved surface if applicable [Contact, 2012]. Also offsetting the adjacent surfaces will account for the material thickness during the simulation, which will avoid the initial penetration.

3.3.3 Hourglassing

LS-DYNA offers hourglass (HG) modes, which are nonphysical and zero-energy modes of deformation. This will produce a zero strain and no stress. The HG effect can

be seen as a deformation of the mesh, which results in zero-energy degrees of freedom. The individual element may appear to have a zigzag or an hourglass shape due to the deformation experienced for that simulation, hence the name hourglass. Hourglassing occurs in under-integrated elements such as solid, shell, and thick-shelled (Tshell) elements. Under-integrated meaning single integration point, and in sold elements this is a single integration point; in shell or Tshells, this is with a single in-plane integration point [Hourglass, 2009]. Single point integration is faster and can be controlled by the various HG algorithms available in LS-DYNA.

Diagnosing the HG effect can be done in several ways. The effect may be seen by inspecting the mesh deformation and can be resolved by decreasing the scale factor. The more reliable way of diagnosing the effect is by directly comparing the energy that is in the zero energy mode to the internal energy of the system. The HG energy should not surpass the internal energy. The algorithms that control the hourglassing in LS-DYNA applies the internal force to resist the hourglass modes. The work done by the internal resisting force calculates the HG energy it takes to resist the hourglass mode and will take away physical energy from the system [Hourglass, 2009].

Hourglassing can be mitigated by using artificial viscosities, using artificial stiffness to the hourglass deformation, refine the mesh and the use of fully integrated elements. Hourglass forces can also be applied in order to resist the hourglass deformation. Not all elements are susceptible to the hourglass mode. Fully integrated elements such as solids and shells do not hourglass because they are more expensive to compute and these elements can be less robust for large deformations. Tetrahedrons and

triangles also do not have hourglassing modes either, but may have stiff behavior depending on the application [Hourglass, 2009].

3.3.4 Post Processing

Once the simulation is successful, post-processing of the model is required. This can be done using LS-PrePost, which is free on the LSTC website [LSTC, 2017]. The desired end result is to create a predicting equation of the maximum Viscous Criterion. As stated in the previous chapter, the surrogate model will be created from the vast number of simulations conducted. Several measurements will have to be taken such as the chest deflection, and the chest deflection velocity in order to calculate the maximum *VC* for each simulation. The maximum *VC* value can be calculated by multiplying the maximum deflection velocity and compression percentage, as seen in *Equation 1.5*. The standard chest thickness for the 50th percentile male crash test dummy is *118.54mm* [Schmitt et al., 2004]. This is measured from the middle of the sternum (*node: 9103*) to the anterior of the thoracic spine (*node: 1787*) as shown in *Figure 3.9*. The compression ratio is the change in compression from the two nodes mentioned above divided by *118.54mm*. For the deflection velocity, a similar approach will be taken by calculating the change in velocity between the two nodes. It should be noted that the impact location should stay consistent through out the different simulation cases. As the impact angle increases, the user should be aware of where the object will impact the chest. If the impact locations are different, then this will create a larger error when producing the predicting equation.
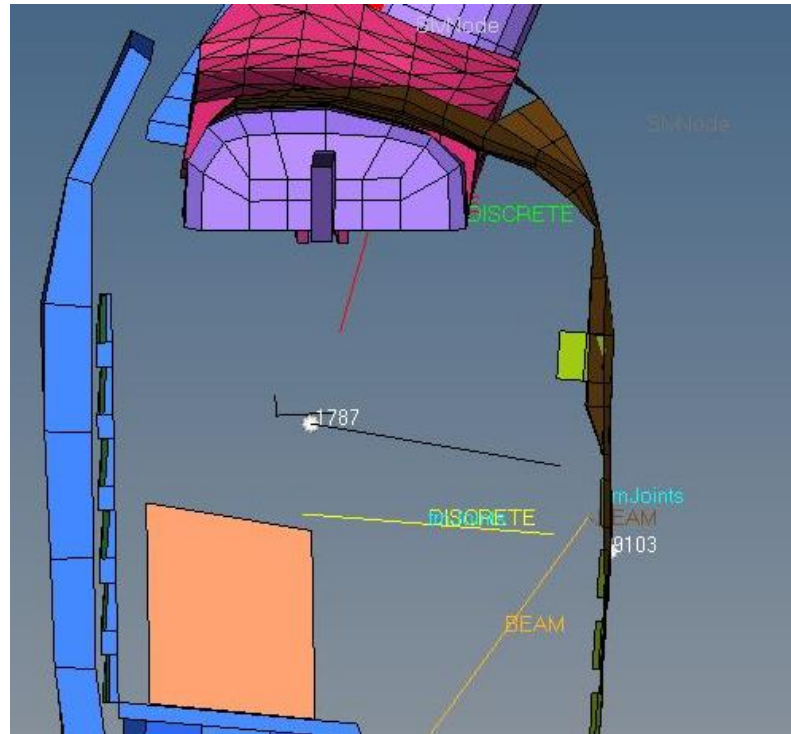
Figure 3.9: Locations of Node 9103 and Node 1787.

To ensure that the simulation results obtained are accurate, an energy check is required. By plotting the total and internal energies, the user will immediately know if there was an error during the simulation. The energy balance is considered to be perfect if the total energy is the sum of the internal energy and the external work, or the energy ratio is equal to one. The energy ratio is the total energy over the sum of the internal energy and the external energy [Total Energy, 2013]. If there is any energy that has dissipated during the simulation, it can be attributed to deleted elements and nodes. Deleted elements are associated with the internal energy, whereas deleted nodes are associated with the kinetic energy. If eroded energy is not present then the energy ration will be equal to one, typically. Deleted elements will have no effect on the total energy/internal energy ratio [Total Energy, 2013].

Positive and negative contact energies should be considered as well when checking the energy ratio. Positive energy contact is expected when friction is included in a contact definition. Friction should result in a positive contact energy if included [Total Energy, 2013]. For the simulations conducted, a static and dynamic friction coefficient of *0.23* and *0.2* respectively, were considered for the automatic single surface contact. Static and dynamic friction coefficient of *0.33* and *0.3* respectively, were considered for a surface-to-surface contact.

If the energy plots show a decrease in in the total energy, a negative contact energy may be the culprit. Negative contact energy may be caused by undetected initial penetration. This can be easily avoided by assuring that the geometry used is carefully defined so that the shells have a proper offset. This is one of the most effective ways to reduce negative contact energy [Total Energy, 2013]. Parts simply sliding with one another can also generate this type of energy. This energy is not friction, but when there is a normal contact force and normal penetration, a node will slide from its original segment into an adjacent unconnected segment. This will cause penetration resulting in negative contact energy. If the internal energy seems to mirror the negative contact energy then it is possible that there is a localized problem. This will have a small impact in the overall simulation validity. Fringing internal energy of the shell part can help in isolating these localized areas. Some other ways to mitigate the negative contact energy are checking and eliminating redundant contact conditions, reducing the time step scale factor, and also eliminating initial penetration as stated earlier [Total Energy, 2013].

Chapter IV: Results

4.1 Surrogate Model

Figures 5.1 and *5.2* shows a typical interaction between the ATD and the sUAS with the parameters: impact angle at *80°*, impact velocity *17 m/s*, and with the mass of *1.372kg* (rotary) and *1.6kg* (fixed). The fringe levels represent the overall displacement experienced by the ATD during the impact. The figures show a step-by-step process of the thoracic impact. The results show the impact causing a large indentation in the chest. Once the contact is complete and the torso and the sUAS are separated, we see that ATD starts a global motion reacting to the impact.
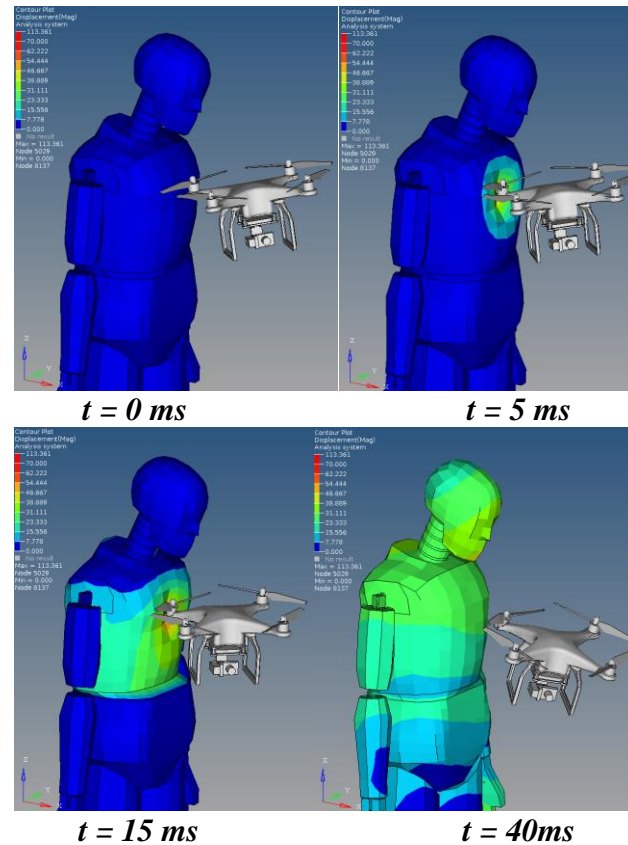
Figure 4.1: A typical interaction between the ATD and the rotary sUAS. (θ=80°, V=17 m/s, M=1.72kg)

t = 0 ms   t = 5 ms

t = 15 ms   t = 40ms
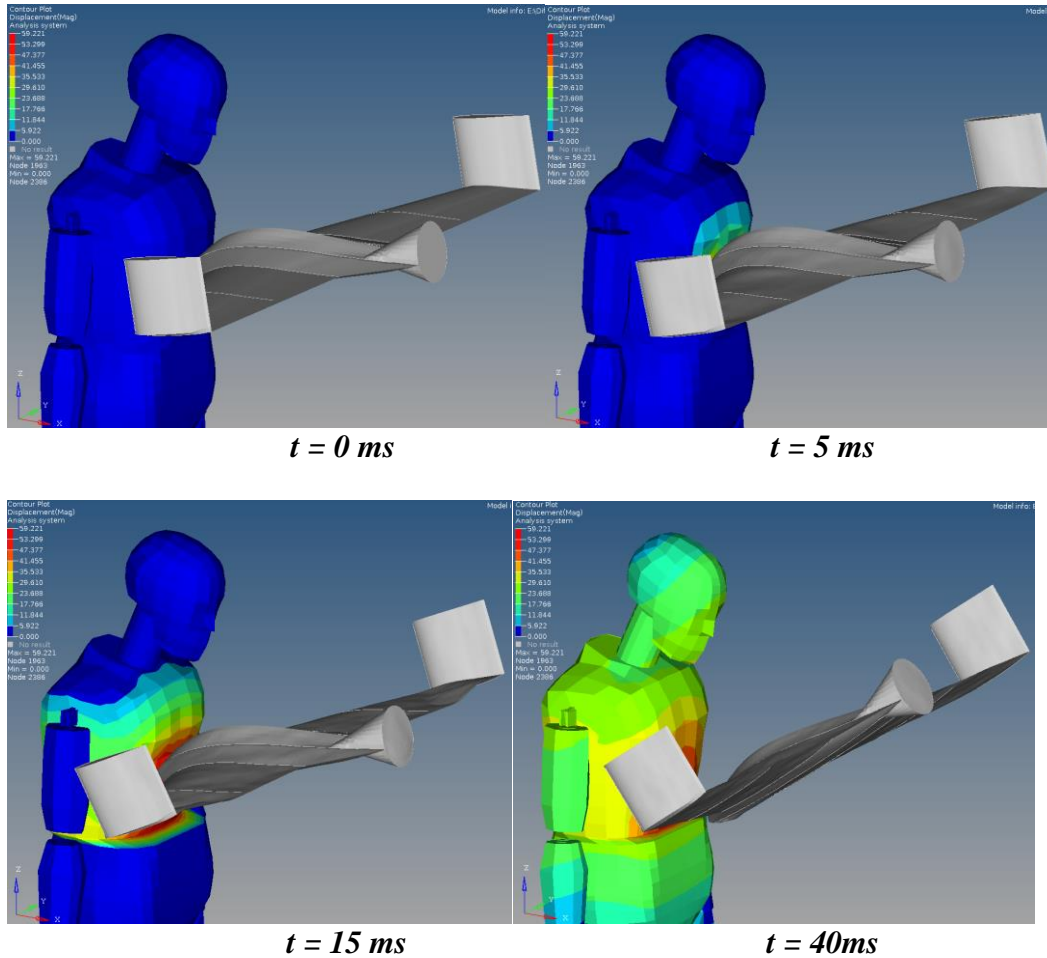
Figure 4.2: *A typical interaction between the ATD and the fixed sUAS. (θ=80°, V=17 m/s, M=1.6kg)*

In order to ensure that the independent variables ($V,\ \theta,\ M$) will contribute in calculating the dependent variable (VC), a correlation analysis was conducted. The results of the Pearson Correlation and the significance for both rotary and fixed wing aircrafts are shown in *Table 4.1* and *4.2,* respectively. From the correlation analysis, we see that the velocity and the impact angle are the most important factors in determining the viscous criterion, VC. This can be confirmed with the significance value as well.

Table 4.1: *Correlation analysis of the independent variables for the Rotary Wing sUAS.*

		Velocity	Angle	Mass
VC	**Pearson Correlation**	0.582779	0.52927	0.186016
	Significance	$3.27*10^{-17}$	$6.00*10^{-14}$	0.0014

Table 4.2: *Correlation analysis of the independent variables for the Fixed Wing sUAS.*

		Velocity	Angle	Mass
VC	**Pearson Correlation**	0.510331	0.589988	0.150564
	Significance	$6.32*10^{-13}$	$1.07*10^{-17}$	0.0474

As mentioned in previous chapters, optimization software called 1stOpt was used to curve-fit the data and approximate the surrogate equation. The coefficients that were determined by the software are shown in *Table 4.3*. The coefficient of correlation is *0.9830* and *0.9755* for the rotary and fixed wing equations respectively. This coefficient shows the relationship between the dependent and independent variables, and thus we see that in both cases they are in good agreement with one another. The determination coefficients for the rotary and fixed wing cases are *0.9663* and *0.9515,* respectively, showing the accuracy of the curve fitting.

Table 4.3: Coefficients for the respective surrogate equations.

	Rotary Wing	Fixed Wing
a	7.48	25.68
b	-24.24	-22.90
c	-46.24	-78.38
d	-2.95	-55.41
e	30.21	36.29
f	9.00	8.06
g	12.65	10.01
h	41.76	25.87
i	120.00	197.25
j	-2.11	62.91
k	-37.79	-19.91
l	-130.02	-185.48
n	0.58	-25.51

4.2 Surrogate Model Verification

Verification of the surrogate model is needed in order to verify the accuracy. Twelve additional cases within each aircraft type were randomly selected and simulated. Once the twenty-four cases were chosen and simulated, the Viscous Criterion's were calculated and compared. The model configurations as well as the response that was calculated by both the numerical simulation and the surrogate model are shown in *Tables 4.4* and *4.5,* respectively for the rotary wing and the fixed wing.

Table 4.4: *Comparing the VC's from the Surrogate model and the Simulations for the Rotary Case.*

| Mass (kg) | Angle (°) | Velocity (m/s) | Viscous Criterion (m/s) | | Percent Difference (%) |
			Surrogate Model	Simulations	
1.084	80	5	0.08	0.07	8.85
1.084	70	20	1.75	1.66	5.18
1.084	50	17	0.49	0.51	3.46
1.084	30	30	0.21	0.21	2.57
1.372	90	14	1.22	1.22	0.04
1.372	80	17	2.00	2.06	2.85
1.372	70	26	3.23	3.52	8.65
1.372	50	11	0.17	0.18	2.26
1.6	90	8	0.35	0.35	0.68
1.6	60	14	1.03	0.95	7.64
1.6	50	23	1.67	1.72	2.54
1.6	30	30	0.43	0.46	4.92

Table 4.5: *Comparing the VC's from the Surrogate model and the Simulations for the Fixed Case.*

| Impact Parameters | | | Viscous Criterion (m/s) | | Percent Difference (%) |
Mass (kg)	Angle (°)	Velocity (m/s)	Surrogate Model	Simulations	
1.084	80	5	2.58	2.51	2.63
1.084	70	20	0.31	0.31	1.17
1.084	50	17	0.36	0.37	3.15
1.084	30	30	0.09	0.09	6.17
1.372	90	14	0.90	0.82	9.49
1.372	80	17	0.11	0.11	2.59
1.372	70	26	0.28	0.27	3.03
1.372	50	11	0.14	0.14	1.85
1.6	90	8	4.50	4.29	4.89
1.6	60	14	2.52	2.62	3.91
1.6	50	23	0.37	0.36	3.61
1.6	30	30	0.09	0.09	3.69

In the rotary wing case, the highest percent difference value that was calculated between the simulated VC and the predicted VC was *8.85%*. For the fixed wing case, the

highest percent difference is *9.49%*. For the fixed wing case, most of the predictions were fairly close to the simulated results, as shown in the table above, when compared to the rotary wing cases. To graphically see the comparison, *Figures 4.3* and *4.4* show the data on a diagonal line whose slope is *1*, representing a perfect correlation.
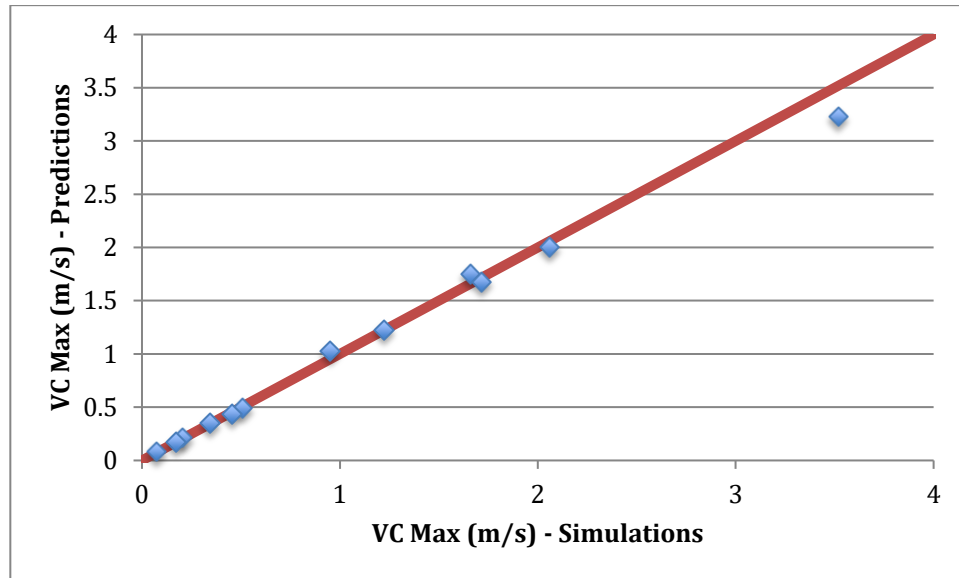
Figure 4.3: *Graphically comparing predicted and simulated results for the Rotary case.*
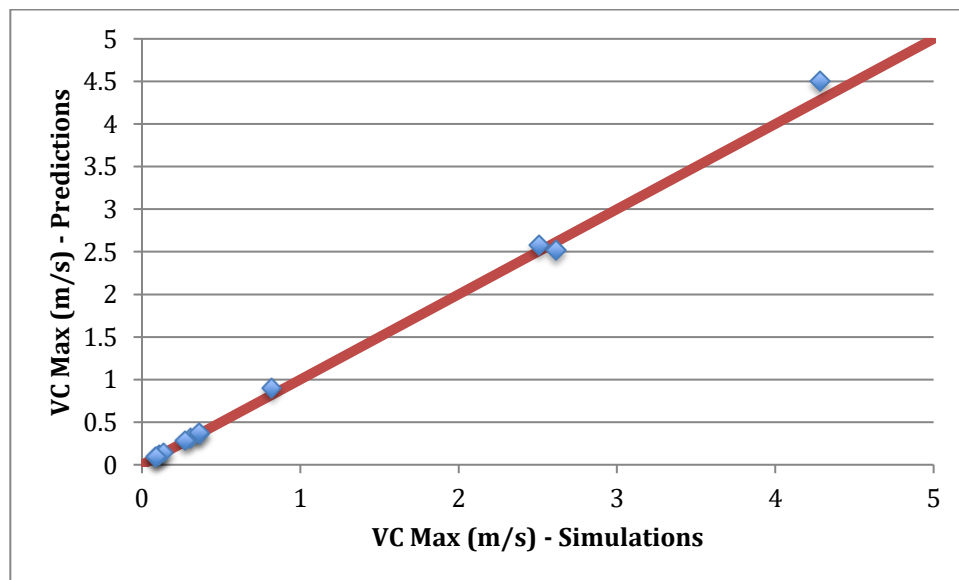
Figure 4.4: *Graphically comparing predicted and simulated results for the Fixed case.*

Chapter V: Discussion, Conclusions, and Recommendations

5.1 Discussion and Limitations

For both aircrafts and the different masses, we see that impact angles of *90°* and *80°* caused the highest VC value. This is primarily due to the sUAS impacting the thorax directly. As the impact angle decreases, the sUAS tends to deflect down the body as seen in *Figure 5.1*. The chest will compress significantly less as well due to the energy being transferred downward rather than directing into the ATD. For example, in *Figure 5.1*, the chest compression experienced by the ATD is *45%* and *18%*, respectively for *90° and 50°*.
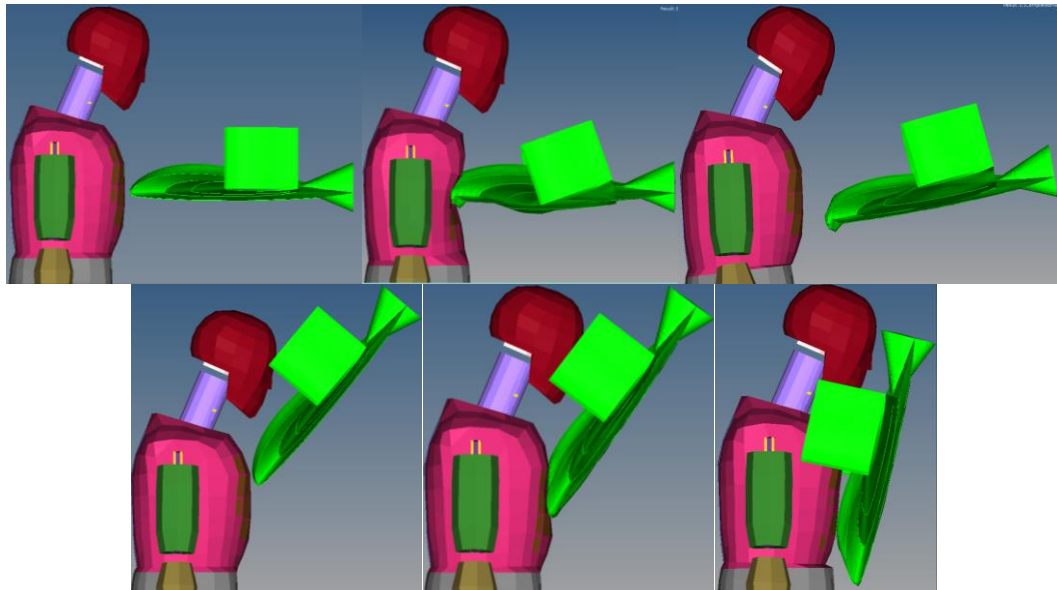
Figure 5.1: *Comparing the sUAS responses.*
Top: *90° Impact at 23 m/s.*
Bottom: *50° Impact at 23 m/s*

For both sUAS types, in the highest mass case (*1.6kg* for rotary and *1.9kg* for fixed wing) an impact angle of *80°* and velocity of *26 m/s* caused the most significant

chest compression of *47%* and *51%,* respectively for rotary and fixed wing. A chest compression of that magnitude will cause *AIS ≥ 4*, which can be very fatal [Viano et al. 1988]. The maximum VC value that was calculated for these cases is *4.8 m/s* and *5.86 m/s*, which is a fatal impact. It is questionable if the aircraft will ever reach those speeds at the impact angle listed above. The maximum velocity for these aircrafts to travel is *16 m/s* and the highest chest compression experienced is roughly *30%,* which is equivalent *Level 1* injury which is equivalent to a AIS *1* rating for the rotary case. For the fixed wing case this was increased to 35% and equivalent *Level 2* injury which is equivalent to a AIS *2-3* rating [Fundamentals, 2017].

As mentioned in the results, the impact velocity and impact angle were more significant in the contribution of calculating the maximum viscous criterion when compared to the mass. When comparing the chest compression ratio between the lightest and heaviest sUAS, there is nearly a *10%* difference in the compression for both aircrafts. This shows that the mass does affect the injury response. Due to the increase in chest compression resulting in a larger VC value, which in turn will correlate to a greater injury to the victim. With this being said, the impact velocity and impact angle still hold a greater significance because as these variables change, the chest compression ratio and the VC value changes along with it.

5.1.1 FE Models

The Hybrid III 50th percentile male ATD is not necessarily a correct depiction of the human thorax. *Figure 5.1* will show a direct comparison between the ATD skeleton and a human body skeleton. It is easily seen that there is some resemblance, but the ATD

is much more robust than an actual human is. The reason for this is the actual purpose of the device. An ATD is built with engineering materials that can withstand multiple high-energy impacts, whereas the human body consists of soft tissue and fragile bones, which cannot withstand repeated impacts. Keeping this in mind, the material selection that is used in impact studies is very important in order to produce an accurate response. The Hybrid III dummies use six high strength steel ribs, which can produce a over-predict the response. Using the correct material characteristics for the human body is currently a challenging task, but it is important to use materials that are similar in order to produce the correct injury response.
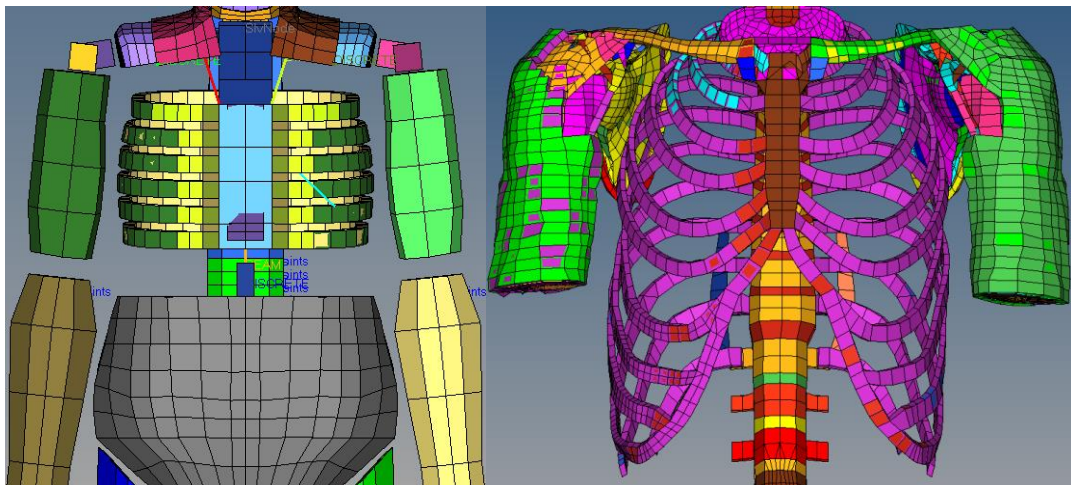
Figure 5.2: Comparison between ATD ribcage and realistic FE ribcage

Human vulnerability itself is dependent on a large number of factors. These factors include the persons posture, clothing, sex, health status, age, height, and weight [Haber et. al, 2005]. The age is a very big factor because this can approximate the condition of their body. For instance, a ten year old child falling off a ledge at five-feet will most likely walk away unharmed when compared to a person in their sixties. A motor-vehicle crash study that was conducted in the UK by Morris et al. examined the

relative injury risk in different age groups. The authors found that older to middle-aged occupants had a greater risk of sustaining AIS *3+* for thoracic injuries. Various amounts of people from different age groups were included in this study [Morris et. al, 2003]. This shows the importance of impact testing for different age groups because the injury response would differ.

5.1.2 Surrogate Equation Limitations

The accuracy of the surrogate equation is dependent on the simplex algorithm that was chosen. This algorithm was chosen for the curve fitting because it can be applied to address problems that have two or more variables. It is also much more desirable than the least-square method, since simplex does not require a derivative function and the orthogonality condition would not be needed. With this in mind, the accuracy of the predicted VC results is highly relied on the curve-fitting algorithm that was chosen.

Currently the surrogate model that is proposed in this paper is a over-predictive model due to the simple fact that the maximum velocities for both of these aircraft are *16 m/s* [DJI]. This maximum velocity is what the aircraft is able to produce on its own traveling on a linear path. Simulations were carried out to either *26 m/s* or *30 m/s*, for each impact angle and mass. The sUAS would impact the user differently during an unexpected descent. For the rotary wing, the aircraft will most likely have an unexpected descent and impact the users head or upper torso region with the aircrafts legs, whereas for the fixed wing, most likely the nose cone will strike the user. So the velocities of the simulations can be reduced significantly to roughly around *20 m/s,* which is roughly *45 mph*. This assumption is highly dependent on the altitude of the sUAS before the user

loses control. If the user is maintaining visual line of sight, as stated in the FAA regulations, then the sUAS should not fall directly onto the user [FAA, 2015].

The number was data points might also have been too low as well. There were seven different angles and eight to nine different velocities that were simulated within each mass case. For each aircraft type, there were only three different masses that were simulated. This can cause the surrogate equation to either over or under-estimate when the user selects a mass that was not simulated. Simulating different mass cases can combat this.

5.2 Conclusion

This research intent was to produce a surrogate model that will involve key impact parameters such as the impact velocity, angle, and the mass of two different types of sUAS models. The sUAS models that were chosen were the Phantom 3 drone, which is a rotary type aircraft, and a GZ500 flying wing, which is a fixed wing aircraft. A vast number of simulations were conducted with varying masses, velocities, and impact angles. From the simulations, the maximum Viscous Criterion was calculated to complete the data set. With the complete data set, a surrogate model was created using normalized mass, normalized velocity, and normalized impact angle as the independent variable; using the calculated max VC as the dependent variable. The purpose of the surrogate equation is to predict the maximum VC without running numerical simulations, which in turn will save computational time and money.

The nonlinear surrogate equations coefficients were approximated using a simplex algorithm. This algorithm was used due its simplicity of application. To verify

the model, twelve respective cases for each aircraft were then selected and a numerical simulation was conducted. These cases have parameters within the dataset, but the data was not used when approximating the surrogate model. The simulation and prediction results were plotted, graphically showing the differences between the two results. Based on the results, the model is in good agreement with the parameters within the data set. The statistical analysis showed that the impact velocity and the impact angle were the two most important factors in predicting the maximum VC.

The current predictive model does have its limitations that originate from the modeling and the curve fitting that was selected. The limitations will cause the predictive model to become over-predictive, and the changes needed to make a more realistic model will be timely task. In the FE sUAS models, internal structures were not modeled in detail for simplicity. There currently is not any experimental data set between sUAS and the chest. As this information may become available, this model can be further modified and verified for improvement.

5.3 Recommendations

Since this is still a relatively new impact study, there are still many ways to improve the surrogate equation so that it is much more realistic. In the following sections, recommendations will be listed in order to improve the validity of the current surrogate equation to ensure the safety of the sUAS users.

5.3.1 ATD Improvements

The first recommendation would be to further improve the biofidelity of the ATD model to achieve a more accurate biomechanical response. As discussed in the Limitation section, the Hybrid III ATD model was originally desired for automotive crashworthiness, therefore using it in other impact scenarios may differ from the desired results. Meaning that building a much more accurate model will be ideal, such as an FE model that has actual organs, skin, and muscles to represent the human body. It is not a simple task to build a more realistic human body model since it is difficult due to the diverse material properties of a human body and also the various number of contacts that will occur during a thoracic impact. Although difficult, using a more realistic human model would be ideal, since the response of the human model will be much more accurate. There are obvious limitations with building a human model, such as the size of the soft tissue, material properties of the soft tissues, stability of the overall model during the impact, and the body composition (since everyone has a different amount of soft tissue, body fat, and muscle mass). If building a human FE model is too challenging with the technology we have now, cadaver testing may be a consideration. Cadaver testing will give much more realistic results than actual simulations. A wide range of body compositions and age must be used to comprise a general expression for the predictive equation.

5.3.2 sUAS Considerations

In this current experiment, only three different masses for each sUAS type were examined. In total, there were *346* different cases that were tested, but there has to be

much more to consider the wider range of masses, velocities, and angles for the different sUAS. The center-of-gravity (CG) location for these models was not considered. The CG location would actually be in a different place when compared to the static location. To further improve the surrogate model, this should be considered. This may seem like an endless task of conducting impact simulations, but the number of cases can be reduced. As discussed in the previous section, the velocities can be reduced to roughly *20 m/s*, which lends the possibility to simulate more cases within a condensed range. This will make the surrogate equation much more robust. As stated earlier, a wider range of mass must be considered as well, and this is so there are more data points for the optimization software to use in order to estimate the surrogate function. By adding a wider range of masses, this can represent the different attachments that the user may have on their specific sUAS.

A wider variety of materials must be considered as well, such as foam. Simulating a foam structure in LS-DYNA is a difficult task, but it is needed to create a much more robust surrogate equation. Majority of fixed wing sUAS are made of foam due to the size and mass constraints. Simulations that will utilize only foam, engineering plastic, and a combination of foam and engineering plastics would be very beneficial. However, this would only be applicable for the fixed wing aircraft, because the rotary wing needs a rigid structure for its engine and rotors.

Different sUAS models must be considered as well since the consumer market for this sector is growing and becoming more popular by the day. It is true that for a quad-rotor, aircraft structures are similar to one another; therefore a single FE model can be used to represent this type of aircraft. As for the fixed winged sUAS, there is much more

of a variety, so different types must be considered. This impact study can be can be branched out to remote-controlled (RC) aircrafts as well since they share a similar structure to that of a fixed wing sUAS. This would mean that, more models must be considered, such as, fixed wing with a rotary engine in the front, fixed wing with a rotary motors on the wing, a RC bi-plane, and much more. By expanding out to different aircraft types, the VC surrogate equation will become much more applicable.

5.3.3 Other Recommendations

As stated in the previous section, the surrogate equation is only as good as the curve-fitting algorithm used. With this in mind, it would be beneficial to explore different types of approximation algorithms such as, Least-Squared Method, Levenverg-Marquardt, or Quasi-Newton. By comparing the results from the different methods, this would eliminate the debate of knowing which algorithm is better suited for this sort of problem.

Meshless methods may also be explored. This is a class of methods that do not require a connection from node to node. These methods do not require interior discretization, integration, polygonalization, and boundaries. The general idea is to minimize or to eliminate the user interaction by automating the process (i.e. solid model to solution in one step). Instead of using a mesh, this is based on the interaction with the neighboring nodes. This method is typically used to find solutions for nonlinear material behaviors, complex 3D geometries, and much more complicated problems; so using this method to approximate a nonlinear equation may be applicable.

In this study, only a thoracic impact was considered. Simulating a rear impact may deem more applicable since the user will not see the sUAS coming towards them. With this being said, the body will able to withstand a posterior impact much better than an anterior impact due to the muscle and skeletal composition [Sturdivan et al., 2004]. Nonetheless, posterior impacts must be explored.

References

Ambrósio, J. A. (2001). *Crashworthiness: energy management and occupant protection*. Wien: Springer.

Athanassiadi, K., Gerazounis, M., & Theakos, N. (2004). Management of 150 Flail Chest Injuries: Analysis of Risk Factors Affecting Outcome. *European Journal of Cardio-Thoracic Surgery, 26*(2), 373-376.

Backaitis, S. H., & St-Laurent, A. (1986). Chest Deflection Characteristics of Volunteers and Hybrid III Dummies. *SAE Technical Paper Series,* 157-166.

Baker, S. P., O'neill, B., Haddon, W., & Long, W. B. (1974). The Injury Severity Score. *The Journal of Trauma: Injury, Infection, and Critical Care,14*(3), 187-196.

Ball, J. A., Knott, M., & Burke, D., Dr. (2012). Crash Lethality Model. *Naval Air Warfare Center Aircraft Division*.

Basic Plastics Education. International Association of Plastics Distributors (IAPD), Retrieved January 05, 2017, http://www.modernplastics.com/technical-resources/basic_plastics_education/

Benson, David. J. The History of LS-DYNA - d3VIEW. Retrieved January 13, 2017, from http://blog.d3view.com/wp-content/uploads/2007/06/benson.pdf

Carsten, O., & O'Day, J. (1984). Injury Priority Analysis. National Highway Traffic Safety Administration,

CDC, Injury in the United States: 2007 Chartbook (March 2008). (2007). Retrieved December 20, 2016, from https://www.cdc.gov/nchs/data/misc/injury2007.pdf

Contact Modeling in LS-DYNA. (November 26, 2012). Retrieved January 14, 2017, from http://www.dynasupport.com/tutorial/ls-dyna-users-guide/contact-modeling-in-ls-dyna

Copes, W. S., Champion, H. R., Sacco, W. J., Lawnick, M. M., Gann, D. S., Gennarelli, T., . . . Schwaitzberg, S. (1990). Progress in Characterizing Anatomic Injury. *The Journal of Trauma: Injury, Infection, and Critical Care,30*(10), 1200-1207.

The Correlation Coefficient. Retrieved March 10, 2017, from http://www.hawaii.edu/powerkills/UC.HTM

Federal Aviation Administration (FAA). Overview of Small UAS Notice of Proposed
    Rulemaking (NPRM) (February 15, 2015). Part 107

Forsgren, A. (2002). Interior Methods for Nonlinear Optimization. *SIAM,44*, 525-597.

Fundamental Principles Of Occupant Protection In Rail Systems. (n.d.). Retrieved
    January 31, 2017, from
    http://www.eurailsafe.net/subsites/operas/HTML/Section3/Section3.3frm.htm

Grez, M. (2015, December 23). Drone almost hits skier. Retrieved December 20, 2016,
    from http://edition.cnn.com/2015/12/23/sport/marcel-hirscher-drone-crash/

Haber JM, Linn AM (2005) Practical Models of Human Vulnerability to Impacting
    Debris. In: First IAASS Conference: "Space Safety, a New Beginning", Nice,
    France, ESA SP-599, pp 543-548

Hourglass. (September 4, 2009). Retrieved January 14, 2017, from
    http://www.dynasupport.com/howtos/element/hourglass

Kallieris, D., Rizzetti, A., & Mattern, R. (1995). The Biofidelity of Hybrid III
    Dummy. *Institute if Legal Medicine,* 135-154.

Kroell, C. K., Schneider, D. C., & Nahum, A. M. (1974). Impact Tolerance and Response
    of the Human Thorax II. *SAE Technical Paper Series.*

Kroell, C. K., Pope, M. E., Viano, D. C., Warner, C. Y., & Allen, S. D. (1981).
    Interrelationship of Velocity and Chest Compression in Blunt Thoracic Impact to
    Swine. *SAE Technical Paper Series*.

Lau, V., & Viano, D. C. (1981). Influence of Impact Velocity on the Severity of
    Nonpenetrating Hepatic Injury. *The Journal of Trauma: Injury, Infection, and
    Critical Care,21*(2), 115-123.

Liberti, L. (February 15, 2008). Introduction to Global Optimization. Lix, Ecole
    Polytechnique, Palaiseau F-91128, France

Lobdell, T. F. (1972). Impact Response of the Human Thorax. *Proceedings of
    Symposium "Human Impact Response Measurement and Simulation,"* General
    Motors Research Laboratories,* 201-245.

LSTC "LS-DYNA Keyword Users Manual" (May 2007) Retrieved January 12, 2017.
    Livermore Software Technoloy Corporation (LSTC). Volume 1 Version 971

Melvin, J. W., Mohan, D., & Stalnaker, R. L. (1975). Occupant Injury Assessment Criteria. *SAE Technical Paper Series*

Melvin, J., & Weber, K. (1985). Review of Biomechanical Response and Injury in the Automotive Environment. U.S. Department of Transportation. National Highway Traffic Safety Administration, Washington, D.C.

Moss, S., Wang, Z., Salloum, M., Reed, M. P., Ratingen, M. V., Cesari, D., Beusenberg, M. (2000). Anthropometry for WorldSID A World-Harmonized Midsize Male Side Impact Crash Dummy. *SAE Technical Paper Series*.

Morris A, Welsh R (2003) Requirements for the Crash Protection of Older Vehicle Passengers. Annu Proc Assoc Adv Automot Med 47:165-180

Neathery, R. F. (1974). Analysis of Chest Impact Response Data and Scaled Performance Recommendations. *SAE Technical Paper Series*.

Phantom 3 Standard - Specs, FAQ, manual, video tutorials and DJI GO - DJI. (n.d.). Retrieved January 08, 2017, from http://www.dji.com/phantom-3-standard/info#specs

Pignolet, F., Duval-Beaupere, G., Guezard, B., Guillon, F., & Tarriere, C. (1990). In Vivo Measurement of Human Weight Supported by the Successive Anatomical Level from C4 to the Femoral Head. *SAE Technical Paper Series*.

Radi, Alexander (2013), Human Injury Model for Small Unmanned Aircraft Impacts. *Civil Aviation Safety Authority/ Monash University.*

Reddy, J. N. (1993). *An Introduction to the Finite Element Method*. New York: McGraw-Hill.

Reddy, J. N. (2006). *An Introduction to the Finite Element Method*. Boston: McGraw-Hill.

Schmitt, K., Niederer, P. F., & Walz, F. (2004). *Trauma Biomechanics: Introduction to Accidental Injury* (2nd ed.). Berlin: Springer.

Simpson, T., Poplinski, J., Koch, P. N., & Allen, J. (2001). Metamodels for Computer-based Engineering Design: Survey and recommendations. *Engineering with Computers,17*(2), 129-150.

Somers, R. L. (1983). The probability of death score: An improvement of the injury severity score. *Accident Analysis & Prevention, 15*(4), 247-257.

Sturdivan, L. M., Viano, D. C., & Champion, H. R. (2004). Analysis of Injury Criteria to Assess Chest and Abdominal Injury Risks in Blunt and Ballistic Impacts. *The Journal of Trauma: Injury, Infection, and Critical Care, 56*(3), 651-663.

Total Energy. (2013, February 3). Retrieved March 11, 2017, from http://www.dynasupport.com/howtos/general/total-energy

Viano, D.C., Lau, V. K., (1983). Role of Impact Velocity and Chest Compression in Thoracic Injury, *Avia Space Environ. Med.,* 16-21

Viano D.C., Lau I.V., (1985), Thoracic Impact: A Viscous Tolerance Criterion, *10th Experimental Safety Vehicle Conference, National Highway Traffic Safety Administration,*104-113

Viano, D. C., Lau, I. V., (1986). The Viscous Criterion - Bases and Applications of an Injury Severity Index for Soft Tissues. *SAE Technical Paper Series*.

Viano, D. C., & Lau, I. V. (1988). A viscous tolerance criterion for soft tissue injury assessment. *Journal of Biomechanics,21*(5), 387-399.

Viano, D. C., Lau, I. V., Asbury, C., King, A. I., & Begeman, P. (1989). Biomechanics of the human chest, abdomen, and pelvis in lateral impact. *Accident Analysis & Prevention,21*(6), 553-574.

Wasserstein, Ronald. Lazar, Nicole. (2016) The ASA's Statement on *p*-Values: Context, Process, and Purpose. *The American Statistician* 70:2, pages 129-133.

"*What are the differences between implicit and explicit?"* (Sept. 19, 2014). Retrieved January 12, 2017, from http://www.dynasupport.com/faq/general/what-are-the-differences-between-implicit-and-explicit

Yoganandan, N., Nahum, A. M., & Melvin, J. W. (2015). *Accidental injury: Biomechanics and Prevention*. New York: Springer.

Models:
Hybrid III Test Dummy
"Download LSTC Dummy and Barrier Models for LS-DYNA." *Welcome to Livermore Software Technology Corp.* N.p., n.d. Web. 15 Oct. 2016.

DJI Phantom 3 Rotary sUAS
Hanmao, J. (2015, August 4). GrabCAD - CAD library. Retrieved January 08, 2017, from https://grabcad.com/library/dji-phantom3-1

GZ500 Fixed Wing sUAS
Niazi, K. (2016, January 6). GrabCAD - CAD library. Retrieved January 08, 2017, from https://grabcad.com/library/gz-500-flying-wing-UAS-ribs-cnc-cad-1

Software:
Optimization Software.
1stOpt Software Package. (2014) http://www.7d-soft.com/

LS-PrePost
Download / Install Overview. Retrieved March 10, 2017, from http://www.lstc.com/download

Appendix A

Finite Element Analysis (FEA) Example

As stated earlier, LS-DYNA is a program that performs finite element analysis, better known as FEA. This numerical technique is used to approximate solutions for boundary value problems with partial differential equations (PDE). This method will subdivide the domain into simpler parts [Reddy, 2006]. By subdividing the domain, we will be able to accurately represent complex geometry much easier, easily represent the solution of a complex problem, able to show the local effects, and also able to use different material properties in the geometry.

The basic concept for solving a finite element problem is to first divide the domain into a series of subdomains. Each subdomain will contain a set of element equations or the original problem. Then is followed by systematically recombining the sets of element equations into a global set of equations then is calculated globally. The global system of equations can be solved using initial values from the original problem to produce a numerical answer [Reddy, 2006].

As stated above, the first step is to divide the original domain into subdomains containing a set of element equations. The element equations are simple equations that will locally approximate the original equation. This step in often times will use the Galerkin Method to construct the polynomial approximation [Reddy, 2006]. The algebraic expression for the Galerkin approximation is shown in *Equation A1*.

$$\sum_{j=1}^{N} A_{ij} c_j = F_i$$

(A1)

Where A_{ij} and F_i are defined by the following:

$$A_{ij} = \int_{\Omega} \phi_i A(\phi_j) dx dy$$

(A2)

$$F_i = \int_{\Omega} \phi_i [f - A(\phi_0)] dx dy$$

(A3)

In *Equations A1* and *A2*, A_{ij} is the basis function and is not symmetric. By using the coefficient c_j, error of the approximation can be minimized. ϕ_i is the weight function and f is the analytical equation [Reddy, 1993]. The Galerkin Method or the weighted residual method is essentially a procedure that will minimize the approximation error by fitting trial functions to the PDE. By fitting the trial functions there will some error that will occur and this is called residual and the polynomial functions or the weight functions, will predict the residuals. This process will approximate the PDE locally by eliminating the spatial derivatives of the PDE. The PDE is approximated locally by the set of ordinary differential equations (ODE) for a transient case and set of algebraic equations for a steady state case, which are both element equations. The set of algebraic equations for a steady state problem is solved using numerical linear algebra methods [Reddy, 2006]. The set of ODE equations for a transient problem are approximated through numerical integration using methods such as Runge-Kutta and Euler's methods.

After this step, the element equations will produce equations for the global system. Transforming the local subdomain nodal coordinates to the global nodes of the domain will generate the global system of equations [Reddy, 2006]. This process is often conducted using FEA software such as LS-DYNA.

To illustrate the concept with FEA, consider a problem to find a circumference of a circle. Summation of the line segment lengths is used to approximate the circumference of the circle. *Figure A1* visually shows the shape and the mesh that is used to approximate of the circumference.
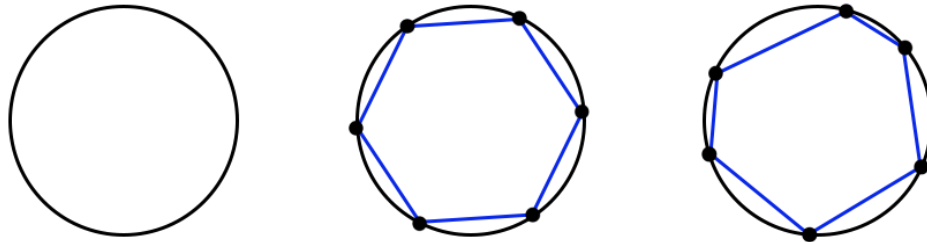
Figure A1*: Different Mesh Examples.*
*(**Left**) Circumference of circle that is being approximated. (**Middle**) Uniform Mesh.*
*(**Right**) Non-uniform Mesh.*

In the first step of a finite element analysis is to divide the domain into finite number of *n*-subdomains or elements, in this case line segments. This is also known as discretization of the domain [Reddy, 1993]. The elements are connected together through nodes, and a collection of elements is called the finite element mesh or mesh. In the example the mesh will have six line segments, *n=6*. It is considered to be a uniform mesh when all of the line segments have the same length, if different then it is called a non-uniform mesh. [Reddy, 1993] *Figure A1* will show both uniform and a non-uniform mesh.

Each element will have its own specific properties; in this case the lengths may vary. The equation that would be used to find the length of the line segment is the equation to find the chord of the circle, shown in *Equation A4*. This will be the computed for each of element in the mesh individually.

$$C_e = 2R \sin \frac{\Theta_e}{2}$$

where: $\Theta_e < \pi$

(A4)

By summing each element equation, we will be able to obtain an approximation of the circumference. *Equation A5* will show a summation of the element lengths. *Cir_n* is the approximate value of the circumference. *Equation A6* will show if C_e were all equal length elements or has a uniform mesh.

$$CIR_n = \sum_{e=1}^{n} C_e$$

(A5)

$$CIR_n = 2nR \sin \frac{\pi}{n}$$

where: $\Theta_e = 2\pi / n$

(A6)

Once the element equations are computed globally the next step is to estimate the error in the system. To estimate the element error, the approximate solution *CIR_n* must converge to *$2\pi R$* with a limit of $n \to \infty$. In this case, the error is approximated by the difference in the sector length and the line segment itself, shown in *Equation A7* [Reddy, 1993],

$$Error_e = |S_e - C_e| = \left[R\Theta_e - 2R\sin\frac{\pi}{n}\right] = 2R\left(\frac{\pi}{n} - \sin\frac{\pi}{n}\right)$$

<div align="right">

(A7)

</div>

From this the global error, *GE* can be calculated by multiplying *Error$_e$* by *n*, shown in *Equation A8.*

$$GE = 2R\left(\pi - n\sin\frac{\pi}{n}\right) = 2\pi R - CIR_n$$

<div align="right">

(A8)

</div>

To complete the convergence, the global error must go to zero as $n \to \infty$. To do this, a limit will be taken of *CIR$_n$,* as shown in *Equation A9.*

$$\lim_{n\to\infty} CIR_n = \lim_{n\to 0}\left(2nR\sin\frac{\pi}{n}\right) = \lim_{n\to 0}\left(2(1)R\cos\frac{\pi}{n}\right) = 2\pi R$$

<div align="right">

(A9)

</div>

This example simply shows that a circumference of a circle can be approximated with *n*-number of piecewise functions. Another important factor to note is that the error decreases as the number of elements is increased [Reddy, 1993]. By having a finer mesh, the approximation of the solution improves, and as the approximation improves the error decreases. Creating a finer mesh will increase the computational load so it isn't wise to use the finest mesh each time.

Appendix B

LS-DYNA Simulation Basics

Every simulation is unique in its own right but there are some general guidelines to follow when preparing FE models for an impact simulation. Some key features to be cautious are keeping consistent units, the keyword inputs, material models used, and boundary conditions to name a few.

Having consistent units is one of the most important characteristics that are commonly overlooked when preparing a simulation. The units must be consistent in order to obtain correct results. The consistent system is defined by *Equations B1, B2,* and *B3*. This shows a simple test to see if a set of units is consistent [LSTC, 2007]. *Table B1* is provided by LSTC to show an example of consistent systems of units.

$$1\ Force\ Unit = 1\ Mass\ Unit * 1\ Acceleration\ Unit$$

(B1)

$$1\ Acceleration\ Unit = \frac{1\ Length\ Unit}{(1\ Time\ Unit)^2}$$

(B2)

$$1\ Density\ Unit = \frac{1\ Mass\ Unit}{(1\ Length\ Unit)^3}$$

(B3)

Table B1: *Consistent System of Units used in LS-DYNA.*

Mass	Length	Time	Force	Stress	Energy	Density (Steel)	Young's Modulus (Steel)	Gravity
kg	m	s	N	Pa	J	7.83e+03	2.07e+11	9.806
kg	cm	s	1.0e-02N			7.83e-03	2.07e+09	9.806e+02
kg	cm	ms	1.0e+04 N			7.83e-03	2.07e+03	9.806e-04
kg	cm	us	1.0e+10 N			7.83e-03	2.07e-03	9.806e-10
kg	mm	ms	kN	Gpa	kN-mm	7.83e-06	2.07e+02	9.806e-03
g	cm	s	dyne	dyne/cm^2	erg	7.83e+00	2.07e+12	9.806e+02
g	cm	us	1.0e+07 N	Mbar	1.0e+07Ncm	7.83e+00	2.07e+00	9.806e-10
g	mm	s	1.0e-06N	Pa		7.83e-03	2.07e+11	9.806e+03
g	mm	ms	N	Mpa	N-mm	7.83e-03	2.07e+05	9.806e-03
ton	mm	s	N	Mpa	N-mm	7.83e-09	2.07e+05	9.806e+03
lbf-s^2/in	in	s	lbf	psi	lbf-in	7.33e-04	3.00e+07	386
slug	ft	s	lbf	psf	lbf-ft	1.52e-01	4.32e+09	32.17
kgf-s^2/mm	mm	s	kgf	kgf/mm^2	kgf-mm	7.98e-10	2.11e+04	9.806e+03
kg	mm	s	mN	1.0e+03 N		7.83e-06	2.07e+08	9.806e+03
g	cm	ms	1.0e+1N	1.0e+05 N		7.83e+00	2.07e+06	9.806e-04

LS-DYNA inputs are called keyword inputs, and provide an organized and flexible database that is simple to understand. Similar functions can be grouped together under the same keyword. The LS-DYNA User Manual has an alphabetically organized keyword section that makes debugging and preparing a simulation much more straightforward. These sections would pertain to a certain input. For instance there are sections for control, material, element, and etc. [LSTC, 2007]. As an example, *Figure B1* will show how flexible the input data can be. This shows how different entities can relate to each other as well as the input organization. It is easily seen that during the preprocessing stage, the program will relate the entities that pertain to that specific

geometry. For more detail, the LS-DYNA User's Manual will provide information of specific details when preparing the geometry for simulation.
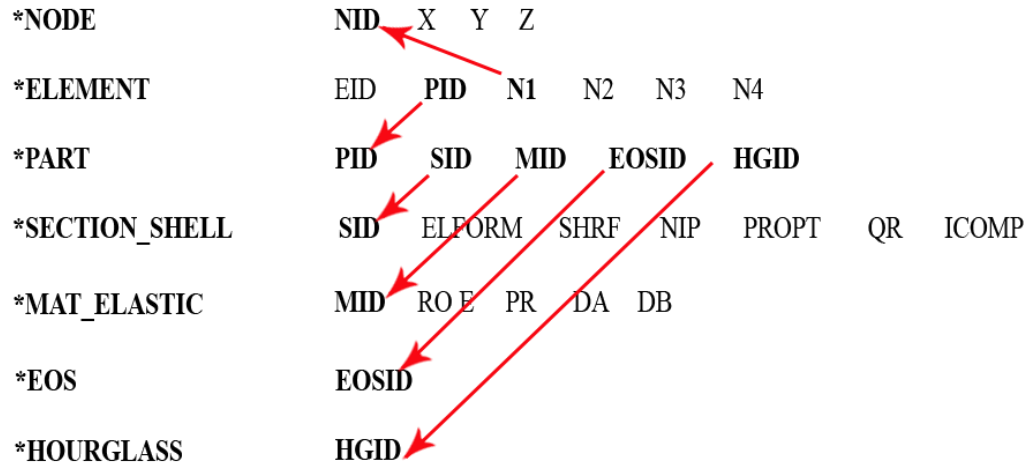
Figure B1: Example of a .k file and how each keyword relates to one another.

Most of the model data can be input in block form. The input data block begins with a keyword followed by the data pertaining to the keyword. The program will go through the keyword data until another keyword is found, which means the end of that data block and the beginning of a new data block. Using data blocks is not required in LS-DYNA, but can make data management must easier [LSTC, 2007]. For instance, the user may group together multiple nodes to assign a loading condition rather than assigning each node the same loading condition multiple times. The input deck is order independent, so there is no need to have the file in a linear order. The keyword is left justified and has an asterisk (*) to denote it. To add a comment, a dollar sign ($) must be added and the program will ignore this line. There is an optional keyword, "*END", which denotes the termination of the file. If this optional keyword is not found at the end

of the .*k file,* then the *END is assumed when it is at end of file. The keyword is not case

sensitive, which makes it easier for the user as well [LSTC, 2007].

A keyword block will typically have multiple input lines and each line in the input

deck is called a "card." Most cards have eight fields with a length of 10 fields as shown

in *Figure B2.* When using the LS-DYNA User Manual, the card details will be shown for

each keyword. Most cards will allow up to eight characters to be used in each field. "F"

will denote a floating point and "I" will denote an integer. If defaults are used then the

code will leave the fields blank, or the card will not be defined [LSTC, 2007].

Card 1	1	2	3	4	5	6	7	8	9	10
Variable	NID	X		Y		Z		TC	RC	
Type	I	F		F		F		F	F	
Default	none	0		0		0		0	0	
Remarks								1	1	

Figure B2: *Card information for keyword *NODE. This card will define the node in the global coordinate system.*

The cards have two different formats that LS-DYNA will accept the inputs as,

Rigid and Free Format. The structures of the rigid and free formats are identical, but the

main difference is how the data is separated. The free format separates the data with

commas, whereas the rigid format separates it with spaces. The free and rigid formats

have the same conditions as described earlier in the card formats. Rigid and free formats

can be mixed together throughout the .*k file* but not within the card itself. *Figure B3*

shows an example of the free format [LSTC, 2007].

*NODE
10101,x,y,z
10201,x,y,z

Figure B3: *Simple *NODE card example in Free Format*

Figure B4 shows the basic input and output scheme of LS-DYNA. The execution syntax and sense switch control commands that further explain each block is shown in the LS-DYNA Users Manual. The execution syntax will provide the user with information that is required for the correct result. The sense switch control commands are commands that can be sent to the solver while it is performing its calculation to check things like estimated time left and, etc. Since every simulation is unique, the desired inputs and outputs are user selected, therefore saving time and memory of the computer.
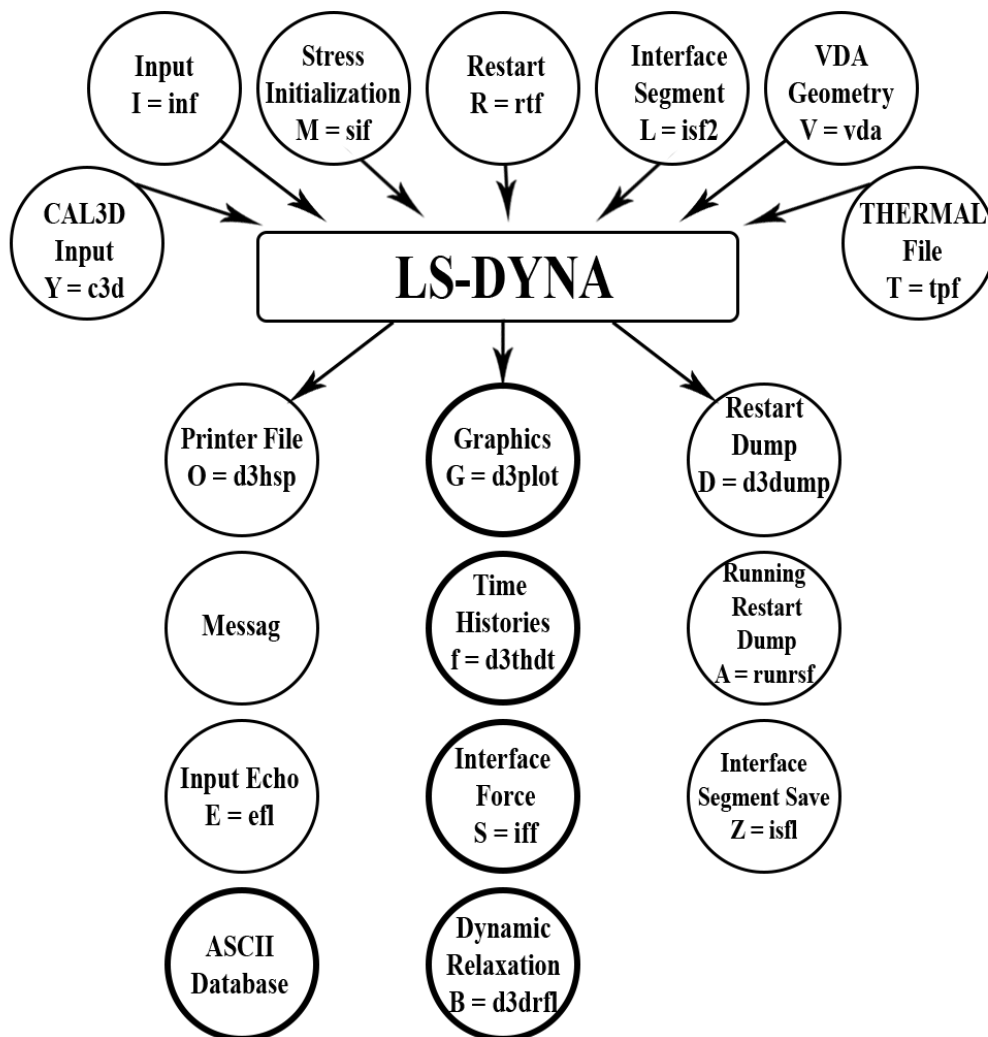
Figure B4: *Flow chart of the input/output scheme in LS-DYNA.*

There are many factors to keep track of when preparing a simulation and hours can be spent on debugging. Some of the most common errors that may cause a sudden interruption include: inconsistent units, incorrect input format, initial penetration, incorrect material properties, and inconsistent loading conditions. Even after a successful run, errors with the model may still arise, such as a numerical error with a boundary condition. Some common errors are the following: units, element size, duplicate node/elements, and incorrect time steps. The user manual and the support website will provide some guidance in how to resolve these issues.

Appendix C

Tables

Table C1: *Phantom 3 Rotary Wing Properties*

Property Name	Keyword	Card Image	Uniform Thickness, T1
Propeller	*SECTION_SHELL	SectShll	2.00
Connection	*SECTION_SHELL	SectShll	2.00
Plate	*SECTION_SHELL	SectShll	2.00
Camera Fixture	*SECTION_SHELL	SectShll	2.00
Camera	*SECTION_SHELL	SectShll	1.00
Camera Bracket	*SECTION_SHELL	SectShll	2.00
Body	*SECTION_SHELL	SectShll	2.00
Leg	*SECTION_SHELL	SectShll	2.00
Rubber Cylinder	*SECTION_SHELL	SectShll	2.00
Engine	*SECTION_SHELL	SectShll	1.00

Table C2: *Phantom 3 Rotary Wing Materials*

Material Name	Card Image	Density (kg/m^3)	Young's Modulus (GPa)
Engineering Plastic	MATL3	1.42e^-6	4.5
Engineering Plastic (Camera)	MATL3	2.68e^-6	66
Engineering Plastic (Engine)	MATL3	2.68e^-6	66

Poisson's Ratio	Yield Strength (MPa)	Static Friction Coefficient
0.3	0.09	0
0.33	0.08	0.18
0.33	0.08	0.18

Table C3: *GZ500 Fixed Wing Properties*

Property Name	Keyword	Card Image	Uniform Thickness, T1
Drone Body	*SECTION_SHELL	SectShll	1.00

Table C4: *GZ500 Fixed Wing Materials*

Material Name	Card Image	Density (kg/m^3)	Young's Modulus (GPA)
Drone	MATL3	1.42e^-6	4.5
Poisson's Ratio	**Yield Strength (MPa)**	**Static Friction Coefficient**	
0.3	0.09	0	

Table C5: *Phantom 3 Rotary Wing Simulation Data*

Mass (kg)	Angle (°)	Velocity (m/s)	Max Deflection (mm)	Max Deflection Velocity (m/s)	Max Calculated VC (m/s)
1.08	90	5	7.11	1.22	0.07
1.08	90	8	11.59	1.92	0.19
1.08	90	11	16.29	2.78	0.38
1.08	90	14	21.38	3.77	0.68
1.08	90	17	26.69	4.92	1.11
1.08	90	20	32.29	6.38	1.74
1.08	90	23	36.72	7.97	2.47
1.08	90	26	39.84	7.84	2.63
1.08	80	5	7.19	1.21	0.07
1.08	80	8	12.07	2.01	0.20
1.08	80	11	16.88	2.77	0.40
1.08	80	14	21.98	3.74	0.69
1.08	80	17	27.56	4.95	1.15
1.08	80	20	33.37	6.20	1.75
1.08	80	23	37.86	7.23	2.31
1.08	80	26	41.22	7.89	2.75
1.08	70	5	6.99	1.18	0.07
1.08	70	8	11.81	1.89	0.19
1.08	70	11	16.62	2.69	0.38
1.08	70	14	21.79	3.59	0.66
1.08	70	17	27.31	4.75	1.09
1.08	70	20	33.20	6.22	1.74
1.08	70	23	38.11	7.05	2.27
1.08	70	26	41.88	7.86	2.78
1.08	60	5	6.41	0.94	0.05
1.08	60	8	10.29	1.61	0.14
1.08	60	11	14.29	2.07	0.25
1.08	60	14	19.21	2.70	0.44
1.08	60	17	25.61	3.83	0.83
1.08	60	20	31.30	5.08	1.34

1.08	60	23	36.23	5.99	1.83
1.08	60	26	39.33	6.65	2.21
1.08	50	5	5.32	0.77	0.03
1.08	50	8	7.94	1.37	0.09
1.08	50	11	9.64	1.43	0.12
1.08	50	14	13.09	2.06	0.23
1.08	50	17	20.30	2.97	0.51
1.08	50	20	24.52	3.92	0.81
1.08	50	23	27.24	4.66	1.07
1.08	50	26	27.60	4.94	1.15
1.08	40	5	3.30	0.61	0.02
1.08	40	8	6.29	1.04	0.06
1.08	40	11	6.29	1.21	0.06
1.08	40	14	7.54	1.43	0.09
1.08	40	17	8.44	1.52	0.11
1.08	40	20	13.08	2.37	0.26
1.08	40	23	17.10	3.25	0.47
1.08	40	26	18.55	3.73	0.58
1.08	40	30	20.66	3.87	0.67
1.08	30	5	3.15	0.56	0.01
1.08	30	8	4.60	0.78	0.03
1.08	30	11	5.17	1.00	0.04
1.08	30	14	5.07	1.03	0.04
1.08	30	17	5.39	1.07	0.05
1.08	30	20	6.21	1.16	0.06
1.08	30	23	7.26	1.21	0.07
1.08	30	26	10.46	1.51	0.13
1.08	30	30	14.40	1.85	0.22
1.37	90	5	9.28	1.33	0.10
1.37	90	8	15.40	2.29	0.30
1.37	90	11	22.10	3.54	0.66
1.37	90	14	29.37	4.83	1.20
1.37	90	17	36.14	6.48	1.98
1.37	90	20	41.03	7.77	2.69
1.37	90	23	45.15	8.72	3.32
1.37	90	26	48.70	9.68	3.98
1.37	80	5	9.45	1.37	0.11
1.37	80	8	15.90	2.34	0.31
1.37	80	11	22.49	3.44	0.65
1.37	80	14	30.19	4.72	1.20
1.37	80	17	37.16	6.46	2.03

1.37	80	20	41.85	7.70	2.72
1.37	80	23	46.44	8.77	3.44
1.37	80	26	50.71	9.35	4.00
1.37	70	5	9.13	1.31	0.10
1.37	70	8	15.41	2.15	0.28
1.37	70	11	22.35	3.30	0.62
1.37	70	14	30.13	4.61	1.17
1.37	70	17	36.93	6.05	1.88
1.37	70	20	42.14	7.70	2.74
1.37	70	23	46.78	7.70	3.04
1.37	70	26	50.63	7.85	3.35
1.37	60	5	8.22	1.08	0.07
1.37	60	8	12.76	1.74	0.19
1.37	60	11	19.12	2.32	0.37
1.37	60	14	26.00	3.50	0.77
1.37	60	17	33.55	5.07	1.43
1.37	60	20	38.76	6.17	2.02
1.37	60	23	42.24	7.25	2.58
1.37	60	26	43.89	7.30	2.70
1.37	50	5	6.65	0.82	0.05
1.37	50	8	9.07	1.40	0.11
1.37	50	11	12.54	1.75	0.19
1.37	50	14	18.11	2.49	0.38
1.37	50	17	22.66	3.43	0.66
1.37	50	20	31.70	5.35	1.43
1.37	50	23	31.34	5.74	1.52
1.37	50	26	28.19	4.72	1.12
1.37	40	5	5.16	0.70	0.03
1.37	40	8	7.48	1.14	0.07
1.37	40	11	6.86	1.26	0.07
1.37	40	14	7.58	1.45	0.09
1.37	40	17	9.46	1.41	0.11
1.37	40	20	10.34	1.76	0.15
1.37	40	23	12.96	1.95	0.21
1.37	40	26	19.63	2.48	0.41
1.37	40	30	23.76	2.52	0.51
1.37	30	5	3.03	0.53	0.01
1.37	30	8	4.92	0.81	0.03
1.37	30	11	5.88	0.99	0.05
1.37	30	14	7.25	1.27	0.08
1.37	30	17	5.74	1.10	0.05

1.37	30	20	6.87	1.07	0.06
1.37	30	23	8.51	1.05	0.08
1.37	30	26	10.85	1.13	0.10
1.37	30	30	13.85	1.23	0.14
1.60	90	5	10.02	1.66	0.14
1.60	90	8	16.65	2.47	0.35
1.60	90	11	24.43	3.77	0.78
1.60	90	14	32.42	5.37	1.47
1.60	90	17	38.79	7.05	2.31
1.60	90	20	43.75	8.28	3.06
1.60	90	23	48.48	9.47	3.87
1.60	90	26	53.52	10.43	4.71
1.60	80	5	10.28	1.49	0.13
1.60	80	8	17.21	2.46	0.36
1.60	80	11	24.61	3.64	0.76
1.60	80	14	33.30	5.65	1.59
1.60	80	17	39.51	7.03	2.34
1.60	80	20	44.59	8.33	3.13
1.60	80	23	49.97	9.54	4.02
1.60	80	26	55.62	10.34	4.85
1.60	70	5	9.95	1.50	0.13
1.60	70	8	16.83	2.30	0.33
1.60	70	11	24.59	3.58	0.74
1.60	70	14	33.12	5.00	1.40
1.60	70	17	39.70	6.74	2.26
1.60	70	20	44.91	8.05	3.05
1.60	70	23	49.92	8.48	3.57
1.60	70	26	51.13	9.38	4.04
1.60	60	5	8.86	1.22	0.09
1.60	60	8	13.36	1.80	0.20
1.60	60	11	21.29	2.49	0.45
1.60	60	14	27.24	4.11	0.94
1.60	60	17	35.88	5.43	1.64
1.60	60	20	41.48	6.84	2.39
1.60	60	23	43.23	7.54	2.75
1.60	60	26	41.88	6.90	2.44
1.60	50	5	6.91	0.95	0.06
1.60	50	8	10.19	1.60	0.14
1.60	50	11	13.28	2.12	0.24
1.60	50	14	18.04	2.53	0.39
1.60	50	17	27.51	3.84	0.89

1.60	50	20	34.47	5.13	1.49
1.60	50	23	37.33	5.43	1.71
1.60	50	26	37.56	5.49	1.74
1.60	40	5	5.37	0.73	0.03
1.60	40	8	8.14	1.28	0.09
1.60	40	11	8.50	1.33	0.10
1.60	40	14	10.02	1.54	0.13
1.60	40	17	14.41	2.12	0.26
1.60	40	20	19.74	3.38	0.56
1.60	40	23	22.89	4.33	0.84
1.60	40	26	24.37	4.25	0.87
1.60	40	30	31.49	4.10	1.09
1.60	30	5	4.12	0.62	0.02
1.60	30	8	5.60	0.92	0.04
1.60	30	11	6.28	1.09	0.06
1.60	30	14	5.75	1.13	0.05
1.60	30	17	7.05	1.20	0.07
1.60	30	20	11.74	1.38	0.14
1.60	30	23	15.21	1.89	0.24
1.60	30	26	16.90	1.97	0.28
1.60	30	30	21.07	2.60	0.46

Table C6: GZ500 Fixed Wing Simulation Data

Mass (kg)	Angle (°)	Velocity (m/s)	Max Deflection (mm)	Max Deflection Velocity (m/s)	Max Calculated VC (m/s)
1.37	90	5	9.49	1.49	0.12
1.37	90	8	15.78	2.49	0.33
1.37	90	11	22.20	3.54	0.66
1.37	90	14	28.45	4.62	1.11
1.37	90	17	34.89	6.00	1.76
1.37	90	20	39.45	7.44	2.48
1.37	90	23	43.39	8.75	3.20
1.37	90	26	47.42	9.00	3.60
1.37	80	5	9.33	1.46	0.11
1.37	80	8	15.20	2.40	0.31
1.37	80	11	20.55	3.41	0.59
1.37	80	14	27.46	4.54	1.05
1.37	80	17	34.56	5.86	1.71
1.37	80	20	38.96	7.17	2.36
1.37	80	23	43.39	8.59	3.14

1.37	80	26	47.76	8.77	3.53
1.37	70	5	8.00	1.28	0.09
1.37	70	8	12.30	2.03	0.21
1.37	70	11	16.88	3.02	0.43
1.37	70	14	20.93	3.78	0.67
1.37	70	17	26.80	4.47	1.01
1.37	70	20	32.26	5.31	1.45
1.37	70	23	36.49	6.29	1.94
1.37	70	26	41.00	7.59	2.63
1.37	60	5	5.89	1.06	0.05
1.37	60	8	8.88	1.67	0.13
1.37	60	11	11.73	2.26	0.22
1.37	60	14	15.48	2.74	0.36
1.37	60	17	17.43	3.12	0.46
1.37	60	20	22.35	4.00	0.75
1.37	60	23	26.21	4.90	1.08
1.37	60	26	31.52	6.04	1.61
1.37	50	5	3.96	0.84	0.03
1.37	50	8	6.27	1.25	0.07
1.37	50	11	8.52	1.66	0.12
1.37	50	14	9.76	1.98	0.16
1.37	50	17	11.40	2.22	0.21
1.37	50	20	13.47	2.58	0.29
1.37	50	23	15.58	2.86	0.38
1.37	50	26	18.00	3.33	0.51
1.37	40	5	2.62	0.52	0.01
1.37	40	8	4.05	0.94	0.03
1.37	40	11	5.96	1.24	0.06
1.37	40	14	7.56	1.63	0.10
1.37	40	17	8.94	1.91	0.14
1.37	40	20	10.66	2.16	0.19
1.37	40	23	12.21	2.44	0.25
1.37	40	26	13.70	2.81	0.32
1.37	40	30	16.55	3.12	0.44
1.37	30	5	1.98	0.37	0.01
1.37	30	8	3.19	0.66	0.02
1.37	30	11	4.63	0.90	0.04
1.37	30	14	5.75	1.20	0.06
1.37	30	17	6.86	1.48	0.09
1.37	30	20	7.94	1.66	0.11
1.37	30	23	9.12	1.88	0.14

1.37	30	26	10.65	2.03	0.18
1.37	30	30	12.48	2.27	0.24
1.60	90	5	10.72	1.64	0.15
1.60	90	8	17.91	2.78	0.42
1.60	90	11	25.51	3.88	0.83
1.60	90	14	32.36	5.23	1.43
1.60	90	17	38.28	6.84	2.21
1.60	90	20	43.14	8.55	3.11
1.60	90	23	47.22	8.99	3.58
1.60	90	26	52.38	9.63	4.26
1.60	80	5	10.63	1.56	0.14
1.60	80	8	17.08	1.96	0.28
1.60	80	11	23.39	3.75	0.74
1.60	80	14	31.42	5.12	1.36
1.60	80	17	38.25	6.56	2.12
1.60	80	20	42.47	8.22	2.94
1.60	80	23	48.04	9.54	3.87
1.60	80	26	53.38	9.80	4.41
1.60	70	5	9.07	1.44	0.11
1.60	70	8	14.03	2.34	0.28
1.60	70	11	19.09	3.33	0.54
1.60	70	14	23.97	4.17	0.84
1.60	70	17	30.80	5.03	1.31
1.60	70	20	37.44	5.94	1.88
1.60	70	23	40.85	7.29	2.51
1.60	70	26	45.09	8.85	3.37
1.60	60	5	6.84	1.15	0.07
1.60	60	8	10.30	1.83	0.16
1.60	60	11	13.19	2.55	0.28
1.60	60	14	17.46	3.06	0.45
1.60	60	17	18.81	3.52	0.56
1.60	60	20	26.30	4.67	1.04
1.60	60	23	29.27	5.59	1.38
1.60	60	26	37.02	7.02	2.19
1.60	50	5	4.53	0.90	0.03
1.60	50	8	7.19	1.35	0.08
1.60	50	11	9.60	1.90	0.15
1.60	50	14	10.75	2.11	0.19
1.60	50	17	13.13	2.48	0.27
1.60	50	20	15.43	2.92	0.38
1.60	50	23	17.87	3.31	0.50

1.60	50	26	20.63	3.78	0.66
1.60	40	5	2.96	0.60	0.02
1.60	40	8	4.69	1.04	0.04
1.60	40	11	6.81	1.31	0.08
1.60	40	14	8.55	1.78	0.13
1.60	40	17	10.19	2.03	0.17
1.60	40	20	11.92	2.39	0.24
1.60	40	23	13.90	2.73	0.32
1.60	40	26	15.89	3.18	0.43
1.60	40	30	18.92	3.44	0.55
1.60	30	5	2.27	0.41	0.01
1.60	30	8	3.66	0.73	0.02
1.60	30	11	5.30	1.02	0.05
1.60	30	14	6.37	1.32	0.07
1.60	30	17	7.48	1.61	0.10
1.60	30	20	9.01	1.80	0.14
1.60	30	23	10.59	2.02	0.18
1.60	30	26	12.16	2.18	0.22
1.60	30	30	14.40	2.46	0.30
1.90	90	5	12.27	1.81	0.19
1.90	90	8	20.45	3.11	0.54
1.90	90	11	28.52	4.29	1.03
1.90	90	14	36.43	5.84	1.80
1.90	90	17	41.91	7.77	2.75
1.90	90	20	47.63	9.40	3.78
1.90	90	23	53.10	9.57	4.29
1.90	90	26	59.47	10.77	5.40
1.90	80	5	12.17	1.68	0.17
1.90	80	8	19.42	2.94	0.48
1.90	80	11	27.13	4.08	0.93
1.90	80	14	35.92	5.65	1.71
1.90	80	17	41.61	7.45	2.62
1.90	80	20	46.96	9.29	3.68
1.90	80	23	54.01	10.28	4.68
1.90	80	26	61.30	11.34	5.86
1.90	70	5	10.36	1.54	0.13
1.90	70	8	16.10	2.62	0.36
1.90	70	11	21.75	3.69	0.68
1.90	70	14	28.57	4.64	1.12
1.90	70	17	35.82	5.69	1.72
1.90	70	20	41.12	6.98	2.42

1.90	70	23	45.32	8.46	3.23
1.90	70	26	49.57	8.90	3.72
1.90	60	5	7.78	1.26	0.08
1.90	60	8	11.69	1.97	0.19
1.90	60	11	15.15	2.83	0.36
1.90	60	14	19.66	3.41	0.57
1.90	60	17	23.66	3.96	0.79
1.90	60	20	29.17	5.09	1.25
1.90	60	23	37.43	7.02	2.22
1.90	60	26	40.87	7.83	2.70
1.90	50	5	5.06	0.98	0.04
1.90	50	8	8.45	1.51	0.11
1.90	50	11	10.77	1.98	0.18
1.90	50	14	12.48	2.34	0.25
1.90	50	17	15.23	2.82	0.36
1.90	50	20	18.43	3.19	0.50
1.90	50	23	21.10	3.74	0.67
1.90	50	26	23.95	4.22	0.85
1.90	40	5	3.38	0.65	0.02
1.90	40	8	5.49	1.11	0.05
1.90	40	11	7.49	1.59	0.10
1.90	40	14	9.81	1.95	0.16
1.90	40	17	11.91	2.31	0.23
1.90	40	20	13.86	2.65	0.31
1.90	40	23	16.09	3.14	0.43
1.90	40	26	18.96	3.43	0.55
1.90	40	30	21.90	3.09	0.57
1.90	30	5	2.64	0.44	0.01
1.90	30	8	4.26	0.83	0.03
1.90	30	11	6.01	1.10	0.06
1.90	30	14	7.28	1.46	0.09
1.90	30	17	8.75	1.76	0.13
1.90	30	20	10.58	19.88	1.77
1.90	30	23	12.07	2.16	0.22
1.90	30	26	14.00	2.41	0.28
1.90	30	30	16.73	2.67	0.38